Heinonen, J.S., Luttinen, A.V., 2008. Jurassic dikes of Vestfjella, western Dronning Maud Land, Antarctica: geochemical tracing of ferropicrite sources. Lithos 105 (3–4), 347–364. http://dx.doi.org/10.1016/j.lithos.2008.05.010 (Author's postprint)

Jurassic dikes of Vestfjella, western Dronning Maud Land, Antarctica: geochemical tracing of ferropicrite sources

Jussi S. Heinonen *, Arto V. Luttinen

Department of Geology, University of Helsinki, P.O. Box 64, 00014 Helsinki, Finland

* Corresponding author. E-mail address: jussi.s.heinonen@helsinki.fi, phone: +358 9 191 50805

Abstract

Ferropicrites and their differentiates make up a geochemically distinctive group of dikes that crosscut Jurassic continental flood basalts of the Karoo large igneous province at Vestfjella, western Dronning Maud Land, Antarctica. The Vestfjella ferropicrites can be divided into two geochemical types: The depleted ferropicrites have $(La/Sm)_N$ of 1.2–1.3, $(Sm/Yb)_N$ of 4.5, initial ε_{Nd} from +7 to +8, initial ε_{Sr} from -18 to -19, and show relative depletion of highly incompatible elements, but pronounced enrichment of V; The enriched ferropicrites have $(La/Sm)_N$ of 1.7, $(Sm/Yb)_N$ of 5.1–5.4, initial ε_{Nd} from +3 to +4, initial ε_{Sr} from 0 to +1, and show general enrichment of incompatible trace elements. The immobile incompatible element signatures of the ferropicrites have not been significantly affected by alteration, fractional crystallization, or contamination. Based on primitive olivine phenocrysts (Fo_{79-88}) and high ε_{Nd} values, the depleted ferropicrites represent near-primary melts derived from anomalous hot mantle sources. Overall, geochemical compositions favor a pyroxenite source for the ferropicrites. Unusually high $(V/Lu)_N$ values of the depleted ferropicrites indicate an affinity to oceanic Fe-Ti gabbros and geochemical modeling favors such a recycled mantle source component in them. The enriched ferropicrites probably represent near-primary melts, but this cannot be confirmed. They may also record an exceptionally Fe-rich source component, but their high Fe contents stem at least partly from relatively low-degree melting at high pressures, as indicated by the high $(La/Sm)_N$ and $(Sm/Yb)_N$ ratios. Examination of a global ferropicrite dataset reveals that the recycled Fe-Ti gabbro component is detectable in many ferropicrites.

Keywords: picrite, large igneous provinces, Karoo, mantle plumes, eclogite, petrology

1. Introduction

Ferropicrites are mildly alkaline to sub-alkaline primitive magmatic rocks (MgO = 12–18 wt. %) characterized by exceptionally high Fe contents (FeO_{tot} > 13 wt. %; Gibson et al., 2000). Ferropicrites were first identified in the 1980's and 1990's in Precambrian volcanic suites in the Fennoscandian (Hanski and Smolkin, 1989, 1995; Hanski, 1992) and Canadian (Stone et al., 1995; Francis et al., 1999) shields, and have been more recently recognized also in several Phanerozoic continental large igneous provinces (LIPs; e.g., Siberian Traps, Karoo, Paraná-Etendeka, North Atlantic Volcanic Province, Madagascar) as relatively low-volume lava flows or dikes (Gibson et al., 2000; Gibson, 2002; Riley et al. 2005). They seem to record a common, albeit minor, magma type, which is confined to early stages of continental LIP magmatism (Gibson, 2002; Riley et al., 2005) and which may indicate a fundamental phase in the evolution of hotspots. Various petrogenetic models have associated ferropicrites with mantle heterogeneities, i.e., streaks of Fe-rich peridotite (Hanski and Smolkin, 1995; Francis et al., 1999; Gibson et al., 2000) or recycled oceanic crust (Gibson 2002; Ichiyama et al., 2006). Most recently, their generation has been ascribed to partial melting of pyroxenite sources during juvenile evolutionary stages of mantle plumes beneath thick continental lithosphere (Tuff et al., 2005). A similar pyroxenite-source, however, has been suggested also for less Fe-rich (FeO_{tot} ≈ 10-12 wt. %) oceanic island basalts

(OIBs) and picrites (OIPs) (Sobolev et al., 2005; Herzberg, 2006). This raises the question as to whether ferropicrites represent distinctive pyroxenite source compositions or melting conditions, or both.

Here we report a previously unknown Karoo-related ferropicrite suite from Vestfjella, western Dronning Maud Land (DML), Antarctica (Fig. 1). The Vestfjella ferropicrites and their magmatic differentiates, designated here as the ferropicritic lineage, are found as dikes crosscutting the adjacent Jurassic CFB lavas and have been recognized as a result of geochemical mapping of the Vestfjella dike swarm. We use high-precision incompatible element and Nd and Sr isotopic data to define the geochemical signature of the Vestfjella ferropicrites and the mantle sources involved. We also evaluate the global ferropicrite dataset in order to identify key factors that facilitate generation of exceptionally Fe-rich melts in some hotspots. Finally, we discuss the implications of ferropicritic magmatism within the context of the Karoo LIP.

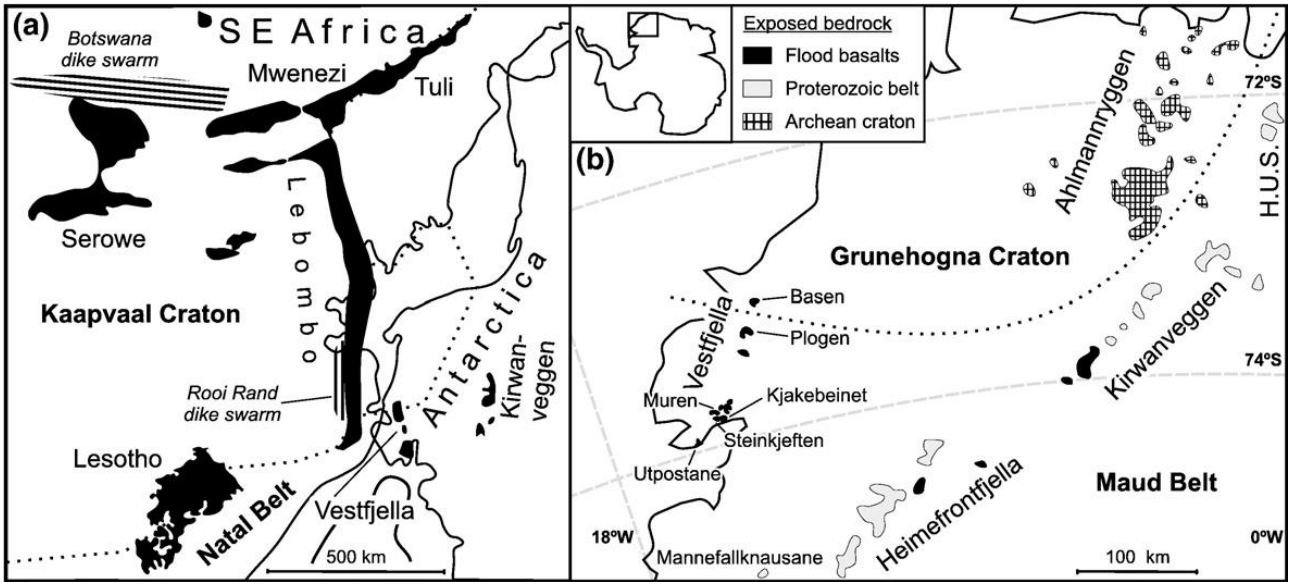

Fig. 1. Distribution of Jurassic continental flood basalts in (a) reconstructed Karoo LIP and (b) western Dronning Maud Land. Gondwana reconstruction in (a) and lithospheric boundary in (b) are after Lawver et al. (1992) and Corner (1994), respectively. H.U.S.=H. U. Sverdrupfjella.

2. Geological setting and field relations

The emplacement of the Middle-Jurassic Karoo LIP was related to the early stages of Gondwana breakup. The peak of magmatic activity has been associated with a relatively short initial period of rifting at 180±4 Ma (Duncan et al., 1997; Jourdan et al., 2007b). The Karoo-related CFBs of western DML represent the uppermost part of the preserved rock strata and overlie Paleozoic sedimentary rocks or the Precambrian basement. The Precambrian basement complex includes two major crustal domains (Fig. 1b): The Archean Grunehogna Craton in the north consists of ~ 3.0 Ga granitic basement (Barton et al., 1987) that is overlain by Proterozoic volcano-sedimentary sequences and intrusive rocks (Wolmarans and Kent, 1982; Moyes et al., 1995). The craton is bounded in the south by the Mesoproterozoic Maud Belt that accreted during the Grenvillian orogeny at ~1100 Ma (Jacobs et al. 1998, 2003).

The CFBs are exposed at Vestfjella, Heimefrontfjella, and Kirwanveggen (Fig. 1b). They form thick stratified lava piles exceeding 900 m in the most voluminous parts at Vestfjella and are geochemically heterogeneous low-Ti basalts (Harris et al., 1990; Luttinen et al., 1998). Intrusive examples of Karoo magmatism are more widespread in western DML. They are highly abundant at Vestfjella, but are also found at Mannefallknausane, Heimefrontfjella, Kirwanveggen, Ahlmannryggen, and H. U. Sverdrupfjella (Fig. 1b). Geochemically, the intrusive rocks vary from

low-Ti types to high-Ti types (Harris et al., 1991; Luttinen et al., 1998; Riley et al., 2005). The high-Ti dikes of Group 3 from Ahlmannryggen consists of high-Fe (FeO_{tot} > 12 wt. %) picrites, including three ferropicrites, and may reveal a plume-related mantle source component in the Karoo LIP (Riley et al., 2005); this component is generally overprinted by lithospheric contamination of the mafic magma types (e.g., Ellam and Cox, 1991; Sweeney et al., 1991; Luttinen et al., 1998; Jourdan et al., 2007a).

Reliable age data for Karoo-related magmatism in DML are sparse. Based on geochemical similarity (Luttinen and Furnes, 2000), geochronological constraints (Peters, 1989; Duncan et al., 1997; Zhang et al., 2003b), and paleomagnetic record (Hargraves et al., 1997; Peters, 1989), the lavas are comagmatic with the ~180 Ma CFBs of southern Africa. Unambiguous $^{40}Ar/^{39}Ar$ age data for the mafic intrusive rocks are limited to a high-Ti Group 4 type sill from Kirwanveggen (Riley et al., 2005) and a low-Ti type gabbro from Utpostane (Vuori and Luttinen, 2003), both dated at 177.0±1.8 Ma using plagioclase (Zhang et al., 2003b), and an ultrapotassic lamproite dike from Vestfjella dated at 158.7±1.6 Ma using phlogopite (Luttinen et al., 2002). All other dated mafic dikes and sills exhibit complex $^{40}Ar/^{39}Ar$ spectra mostly with anomalous >200 Ma low- and high-temperature fractions suggestive of excess ^{40}Ar (Zhang et al., 2003b; Riley et al., 2005). One of the Group 3 dikes at Ahlmannryggen records ~190 Ma mid-temperature fractions (whole-rock) that have been interpreted to indicate emplacement of high-Fe picrites during the initial stages of Karoo magmatism (Riley et al., 2005). Correlation of the intrusive rocks types with the lavas is further hampered by the geochemical differences and the lack of crosscutting field relationships outside Vestfjella (Harris et al., 1991; Zhang et al., 2003b; Riley et al., 2005).

The ferropicritic lineage of Vestfjella mainly comprises ~1–10 m wide dikes that crosscut CFB lavas in N-S or NE-SW directions at Basen, Muren, Kjakebeinet, Steinkjeften, and Utpostane (Fig. 1b). One of the dikes crosscuts a gabbroic intrusion at Muren. Extrusive equivalents of ferropicrites are not known (Luttinen and Furnes, 2000). A subset of samples consists of glacial boulders found abundantly on Basen. Some of the boulders contain chilled, crosscutting margins against sandstone. The total number of dikes is 11, but, in places, spatial correlation is hampered by poor exposure. Recent $^{40}Ar/^{39}Ar$ incremental heating dating of plagioclase in one of the ferropicrite samples from Basen (AL/B16-98) yielded a discordant integrated age of ~193 Ma and an "error plateau" age of ~164 Ma (Zhang et al., 2003b). The older age is attributable to excess ^{40}Ar in several high- and low-temperature fractions typified by exceptionally low K/Cl values and apparent ages of >200 Ma (Zhang et al., 2003b). The younger age represents ~47 % of the total ^{39}Ar released and does not correspond to any reliably dated phase of Karoo magmatism (cf. Jourdan et al., 2007b).

3. Analytical methods

Geochemical whole-rock compositions were analyzed for 28 hand-sized samples that were extracted from the bedrock and glacial boulders. Some samples represent different parts of the same dike. The samples were ground in a steel jaw crusher and the freshest chips were handpicked for analyses to avoid weathered surfaces and contamination with preparation equipment. The XRF and ICP-MS analyses were performed at the Geoanalytical Laboratory, Washington State University. Technical notes and principles of these methods have been described by Johnson et al. (1999) and Knaack et al. (1994), respectively. The geochemical data for the ferropicritic lineage together with the result for international standard BCR-1 are listed in Table 1. Repeated analyses of BCR-1 indicate high precision in general, although coefficients of variation for Cu (16.7 %), Th (9.5 %), and U (9.3 %) are relatively high. Comparison of results for BCR-1 standard with recommended values demonstrates good accuracy for both analytical methods. The poor accuracy of Cr analysis reflects low concentration in the standard sample: The accuracy for reference samples with higher Cr contents (> 30 ppm) is good (Johnson et al., 1999).

Heinonen, J.S., Luttinen, A.V., 2008. Jurassic dikes of Vestfjella, western Dronning Maud Land, Antarctica: geochemical tracing of ferropicrite sources. Lithos 105 (3–4), 347–364.
http://dx.doi.org/10.1016/j.lithos.2008.05.010 (Author's postprint)

Table 1
Whole-rock geochemistry of the Vestfjella ferropicritic lineage

Sample	AL/ B20a-98	14- KHG-90*	AL/ B17-98	AL/ B4-98	22- KHG-90*	AL/ B7-98	117- KHG-91	AL/ B13a-98	AL/ B13b-98	AL/ B14e-98	AL/ B16-98	AL/ WM1b-98	AL/ WM1c-98	AL/ WM1e-98	AL/ WM3a-03	AL/ WM3b-03
Type	E-FP	E-FP	E-FP	E-FP	E-FP	E-FP	D-FP	D-FP	D-FP	D-FP	D-FP	D-FP	D-FP	D-FP	D-FP	D-FP
Dike	1(cm)	1	2(cm)	2(cm)	2	2	3	4(cm)	4	4	4	5(cm)	5	5	5	5
Width(m)	1.0	1.0	2.0	2.0	2.0	2.0	10.0	2.0	2.0	2.0	2.0	1.0	1.0	1.0	1.0	1.0
Strike (º)	030	030	010	010	010	010	030	010	010	010	010	035	035	035	035	035
Lat. (S)	73º01'46"	73º01'50"	73º02'09"	73º01'14"	73º01'04"	73º01'18"	73º46'23"	73º01'18"	73º01'18"	73º01'18"	73º01'22"	73º43'49"	73º43'49"	73º43'49"	73º43'49"	73º43'49"
Long.(W)	13º25'10"	13º25'18"	13º25'06"	13º23'50"	13º23'38"	13º23'56"	14º56'38"	13º21'47"	13º21'47"	13º21'47"	13º21'52"	15º06'10"	15º06'10"	15º06'10"	15º06'10"	15º06'10"
Locality¤	Basen	Basen	Basen	Basen	Basen	Basen	Stk	Basen	Basen	Basen	Basen	WM	WM	WM	WM	WM
Major and minor elements (wt. %, normalized to 100% volatile free)																
SiO_2	44.94	44.87	49.95	48.31	49.53	49.07	43.74	46.14	45.66	46.75	45.38	44.60	44.07	43.65	43.84	44.18
TiO_2	3.41	3.21	3.04	3.17	3.14	3.16	3.31	2.89	2.58	2.49	2.47	2.43	2.14	2.07	2.08	2.14
Al_2O_3	9.27	8.59	10.99	11.47	11.06	11.29	11.63	10.53	8.86	8.58	8.76	10.54	9.13	8.85	8.88	9.18
FeO_{tot}	15.50	17.03	13.16	14.31	12.97	13.69	16.59	12.88	13.99	15.03	14.62	14.38	14.37	15.10	14.44	14.51
MnO	0.18	0.31	0.15	0.18	0.17	0.18	0.21	0.17	0.20	0.24	0.20	0.20	0.20	0.20	0.20	0.20
MgO	12.84	14.27	10.16	10.54	11.08	10.49	11.31	14.81	18.09	15.75	16.71	14.52	18.65	18.88	19.47	18.46
CaO	11.37	9.53	9.85	8.56	9.51	9.37	10.20	10.88	9.38	9.42	9.74	10.59	9.24	9.02	8.99	9.02
Na_2O	1.48	1.26	1.94	1.96	1.62	1.76	1.60	1.19	0.85	1.31	1.63	1.68	1.50	1.53	1.43	1.40
K_2O	0.59	0.53	0.37	1.07	0.54	0.59	1.00	0.25	0.17	0.21	0.28	0.85	0.51	0.50	0.48	0.72
P_2O_5	0.42	0.39	0.39	0.42	0.37	0.39	0.41	0.25	0.22	0.20	0.21	0.23	0.19	0.19	0.19	0.19
LOI	4.40	5.45	3.68	4.46	4.56	3.86	1.67	4.86	6.45	3.76	1.07	1.93	1.25	1.58	1.30	2.24
Total***	99.33	-	99.82	100.06	-	99.30	98.49	98.95§	99.67	98.29§	99.55	100.10	98.76§	99.62	98.34§	98.67§
Mg#**	62	62	60	59	63	60	57	69	72	67	69	67	72	71	73	72
Trace elements (ppm)																
Cr(XRF)	529	549	352	361	370	357	410	727	929	1184	931	1052	1101	1022	1099	1087
Ni	526	696	338	350	367	370	375	569	974	938	732	587	856	880	897	842
V	311	319	263	263	284	258	487	428	397	387	401	421	375	364	361	373
Zr	171	159	156	170	153	160	202	150	138	124	131	121	104	104	102	103
Ba (ICP)	154	176	140	715	186	165	326	42	26	38	51	93	81	91	76	115
Rb	11.61	14.20	6.92	18.06	8.50	7.85	22.40	4.47	4.33	6.84	6.84	13.09	8.71	8.39	8.37	11.23
Sr	355	391	455	246	392	404	768	237	180	273	321	292	281	303	270	313
Ta	1.44	1.38	1.25	1.28	1.24	1.23	1.00	0.66	0.59	0.56	0.62	0.49	0.45	0.43	0.43	0.45
Nb	21.29	20.40	17.55	18.05	19.70	17.06	17.22	8.97	8.25	7.54	9.10	6.84	6.08	6.05	5.95	5.98
Sc	26	26	21	22	26	21	36	30	28	29	30	30	23	28	22	24
Hf	4.44	4.33	4.16	4.45	4.37	4.10	5.18	4.02	3.53	3.39	3.53	3.10	2.90	2.74	2.81	2.79
Y	28.37	28	28.27	30.06	27	28.22	27.85	22.66	20.62	18.35	20.05	19.00	16.25	16.65	15.55	15.92
Th	1.90	1.33	1.86	2.01	1.70	1.86	1.83	0.90	0.74	0.66	0.86	0.57	0.52	0.49	0.49	0.49
U	0.48	0.52	0.47	0.50	0.52	0.46	0.48	0.26	0.22	0.19	0.21	0.18	0.15	0.15	0.14	0.15
La	21.17	21.10	18.06	18.15	18.35	17.88	23.27	12.62	10.96	10.39	11.38	9.08	8.32	7.75	7.91	8.02
Ce	46.07	44.60	38.84	40.34	38.99	38.20	52.28	34.30	28.68	28.46	29.12	23.07	22.57	19.78	21.48	21.75
Pr	6.01	5.90	5.08	5.31	5.16	4.99	7.00	5.15	4.11	4.34	4.15	3.32	3.50	2.88	3.33	3.40
Nd	28.27	27.09	23.84	25.20	24.34	23.49	32.61	24.08	19.71	20.18	19.91	16.67	16.71	14.51	16.01	16.36
Sm	7.90	7.62	7.12	7.58	7.27	7.10	8.26	6.11	5.43	5.14	5.43	4.91	4.64	4.32	4.30	4.44
Eu	2.91	2.51	2.62	2.75	2.64	2.61	2.77	2.32	1.98	1.71	1.89	1.72	1.63	1.52	1.55	1.55
Gd	8.05	7.40	7.67	8.25	7.63	7.55	7.95	6.13	5.36	5.19	5.42	5.05	4.64	4.46	4.59	4.62
Tb	1.23	1.17	1.19	1.25	1.22	1.18	1.17	0.94	0.84	0.78	0.82	0.78	0.71	0.68	0.69	0.70
Dy	6.59	6.35	6.46	6.98	6.46	6.51	6.29	5.30	4.66	4.35	4.53	4.39	3.99	3.79	3.81	3.88
Ho	1.15	1.09	1.13	1.18	1.14	1.11	1.06	0.95	0.83	0.77	0.82	0.77	0.70	0.68	0.67	0.69
Er	2.53	2.49	2.50	2.69	2.59	2.52	2.44	2.23	1.98	1.81	1.90	1.74	1.63	1.54	1.56	1.60
Tm	0.31	0.31	0.31	0.33	0.30	0.30	0.31	0.29	0.25	0.23	0.24	0.23	0.20	0.20	0.20	0.20
Yb	1.58	1.63	1.59	1.70	1.59	1.59	1.81	1.56	1.35	1.25	1.30	1.19	1.13	1.06	1.06	1.08
Lu	0.22	0.23	0.22	0.23	0.22	0.22	0.25	0.22	0.20	0.18	0.18	0.17	0.16	0.15	0.14	0.15

Table 1 continued

Sample	AL/ KB5-98	AL/ KB17-98	MHR-1	X2- KHG-90	X6- KHG-90	128- KHG-91	AL/ B1a-03	AL/ B1b-03	AL/ B3-03	AL/ B5-03	AL/ B7-03	AL/ B8a-03	AL/ B8b-03	AL/ B9-03	BCR-1 †	BCR-1 ‡
Type	D-FP	D-FP	D-FP	D-FP	D-FP	D-FP	D-FP	D-FP	D-FP	D-FP	D-FP	D-FP	D-FP	D-FP	basalt	basalt
Dike	6	7	8	9	10	11	blder1(cm)	blder1	blder2	blder3	blder4	blder5	blder5	blder6	STD	STD
Width(m)	4.0	?	8.0	1.5	1.0	1.0	-	-	-	-	-	-	-	-		
Strike (º)	045	050	050	070	045	050	-	-	-	-	-	-	-	-		
Lat. (S)	73º47'02"	73º47'30"	73º43'40"	73º55'03"	73º55'25"	73º43'43"	73º02 30	73º02 30	73º02'30"	73º02'30"	73º02'30"	73º02'30"	73º02'30"	73º02'30"		
Long.(W)	14º52'22"	14º50'30"	15º02'26"	15º33'44"	15º38'09"	15º02'09"	13º24 00	13º24 00	13º24'00"	13º24'00"	13º24'00"	13º24'00"	13º24'00"	13º24'00"		
Locality¤	Kb	Kb	EM	Up	Up	EM	Basen	Basen	Basen	Basen	Basen	Basen	Basen	Basen		
Major and minor elements (wt. %, normalized to 100% volatile free)															WSUGeolab	reference
SiO_2	46.53	46.51	47.96	47.56	45.31	46.88	52.70	46.57	48.28	45.46	47.05	45.00	44.07	45.53	55.54 (0.0)	55.22
TiO_2	3.01	3.02	1.53	4.02	2.61	2.66	2.37	1.61	2.62	1.59	1.70	1.57	1.31	1.44	2.29 (0.4)	2.29
Al_2O_3	13.81	13.83	11.01	12.67	14.36	13.85	11.91	8.31	10.66	7.09	8.59	6.84	5.77	7.01	13.76 (0.1)	13.92
FeO_{tot}	15.59	15.92	10.79	16.05	15.69	15.99	15.32	13.14	13.02	13.21	12.87	13.20	13.45	12.74	12.16 (0.2)	12.32
MnO	0.19	0.23	0.19	0.23	0.19	0.22	0.22	0.20	0.19	0.20	0.20	0.20	0.20	0.19	0.19 (0.4)	0.18
MgO	6.20	6.16	16.52	5.12	6.80	6.16	10.01	19.21	12.98	23.81	18.57	24.15	27.52	24.39	3.49 (1.4)	3.55
CaO	11.70	10.78	9.40	10.17	12.09	11.36	5.77	9.09	9.96	7.13	9.24	7.38	6.28	7.14	7.12 (0.2)	7.09
Na_2O	2.34	2.81	1.24	3.03	2.51	2.39	1.34	1.41	1.82	1.11	1.41	1.31	1.06	1.31	3.34 (1.3)	3.34
K_2O	0.39	0.49	1.21	0.70	0.20	0.27	0.20	0.34	0.26	0.26	0.23	0.23	0.23	0.15	1.75 (0.2)	1.72
P_2O_5	0.24	0.24	0.17	0.46	0.24	0.22	0.18	0.12	0.22	0.13	0.13	0.13	0.11	0.11	0.37 (0.3)	0.37
LOI	1.79	1.34	-	0.28	0.70	0.87	7.38	1.55	2.68	1.78	1.23	0.68	1.07	1.04		
Total***	98.62	98.10§	96.94	98.74	98.00	98.47	97.79§	99.25§	97.96§	97.82§	98.50§	98.38§	98.26§	98.00§		
Mg#**	44	43	75	39	46	43	56	74	66	78	74	78	80	79		
Trace elements (ppm)															WSUGeolab	reference
Cr(XRF)	85	55	980	89	123	68	965	1211	988	1275	1132	1400	1512	1252	27 (3.6)	16
Ni	97	95	684	50	117	78	433	848	634	1193	807	1256	1481	1270	0 (0)	13
V	557	528	300	585	494	516	396	306	448	280	321	283	237	265	405 (1.7)	407
Zr	131	124	102	246	125	123	104	77	132	81	80	80	66	69	176 (0.6)	190
Ba (ICP)	128	160	313	268	116	110	83	106	49	66	56	56	37	25	672 (1.9)	681
Rb	4.63	6.30	26.00	14.20	3.20	2.70	4.91	9.19	5.27	7.26	6.67	4.88	5.69	3.57	48.1 (1.4)	47.2
Sr	395	437	284	441	479	422	335	251	282	225	242	222	180	188	328 (0.0)	330
Ta	0.53	0.55	0.41	1.00	0.50	0.40	0.53	0.39	0.49	0.40	0.41	0.41	0.34	0.26	0.85 (2.7)	0.81
Nb	7.58	7.76	6.40	16.49	8.76	7.35	7.07	5.22	6.68	5.20	5.55	5.54	4.55	3.46	11.88 (2.2)	14.0
Sc	30	29	29	30	30	31	33	26	28	22	28	25	21	23	X (x)	33
Hf	3.44	3.53	2.62	6.76	3.45	3.36	2.91	2.10	3.58	2.20	2.19	2.13	1.73	1.85	4.93 (1.5)	4.95
Y	22.41	20.67	17.78	40.20	22.10	21.53	19.13	14.05	21.17	13.57	15.10	13.29	10.68	12.81	37.78 (0.8)	38
Th	0.80	0.77	0.42	1.28	0.56	0.63	0.61	0.43	0.60	0.46	0.45	0.48	0.38	0.32	6.26 (9.5)	5.98
U	0.21	0.20	0.14	0.43	0.17	0.20	0.18	0.13	0.19	0.14	0.14	0.16	0.12	0.10	1.63 (9.3)	1.75
La	12.13	11.67	7.53	21.45	11.53	10.78	9.78	7.06	10.18	7.11	7.53	7.84	6.28	5.48	25.86 (1.9)	24.9
Ce	29.54	29.87	16.69	53.02	28.04	26.70	26.09	18.74	28.22	19.04	20.05	20.75	16.63	15.09	53.05 (1.2)	53.7
Pr	4.20	4.47	2.40	7.59	4.08	3.91	3.86	2.79	4.38	2.83	2.97	3.02	2.43	2.32	7.05 (1.0)	6.8
Nd	20.91	21.40	12.15	37.16	19.58	19.01	17.94	12.91	20.89	13.06	13.83	13.57	11.07	11.15	28.87 (1.8)	28.8
Sm	5.88	5.60	3.67	10.25	5.42	5.29	4.67	3.42	5.51	3.43	3.64	3.44	2.76	3.05	6.86 (2.1)	6.59
Eu	2.17	2.03	1.33	3.34	1.95	1.88	1.22	1.19	1.89	1.19	1.28	1.18	0.95	1.11	2.00 (2.5)	1.95
Gd	5.85	5.70	3.91	10.21	5.62	5.42	4.77	3.54	5.70	3.47	3.73	3.46	2.72	3.17	6.90 (1.1)	6.68
Tb	0.91	0.86	0.63	1.58	0.89	0.84	0.76	0.55	0.88	0.55	0.59	0.53	0.44	0.51	1.09 (1.1)	1.05
Dy	5.05	4.80	3.69	8.78	4.81	4.70	4.41	3.23	4.93	3.14	3.41	3.03	2.49	2.93	6.34 (1.3)	6.34
Ho	0.91	0.85	0.69	1.59	0.87	0.86	0.82	0.60	0.89	0.58	0.63	0.55	0.45	0.55	1.26 (1.5)	1.26
Er	2.09	2.08	1.58	3.73	2.09	2.05	1.94	1.46	2.14	1.42	1.56	1.33	1.12	1.30	3.62 (1.4)	3.63
Tm	0.28	0.27	0.22	0.48	0.28	0.28	0.26	0.20	0.28	0.18	0.20	0.18	0.14	0.17	0.53 (1.2)	0.56
Yb	1.56	1.49	1.26	2.79	1.52	1.49	1.48	1.08	1.55	1.01	1.15	0.98	0.82	0.95	3.33 (0.9)	3.38
Lu	0.22	0.22	0.19	0.39	0.21	0.22	0.22	0.16	0.22	0.15	0.16	0.14	0.12	0.14	0.50 (1.9)	0.51

For trace elements from Cr to Zr XRF-values given; for trace elements from Ba to Lu ICP-MS values given; cm = chilled margin; blder = boulder sample; STD = standard; * Data from Luttinen et al. (1998); ** Mg-number [atomic $Mg/(Mg+Fe^{2+})$; $Fe^{2+}/Fe_{tot} = 0.9$]; *** Total prior to normalization; § LOI included in Total; ¤ Abbreviations of localities: Stk = Steinkjeften, WM = West-Muren, Kb = Kjakebeinet, EM = East-Muren, Up = Utpostane; † Washington State University GeoAnalytical Lab standard (BCR-1) analysis (average; coefficient of variation for repeated analyses of corresponding sample BCR-P presented in parentheses); X = no given value; ‡ Recommended values for BCR-1 (after Govindaraju, 1994).

The isotopic analyses were performed at the Unit for Isotope Geology, Geological Survey of Finland. The rock powders were dissolved in molded Teflon vials in a 1:4 mixture of HNO_3 and HF. After evaporation, the samples were dissolved in HCl and a solution spiked with a ^{149}Sm-^{150}Nd tracer. Strontium and light rare earth elements (REE) were separated using standard cation exchange chromatography, after which Sm and Nd were purified on quartz columns. Isotopic ratios of Sr, Sm, and Nd and concentrations of Sm and Nd were measured on a VG Sector 54 mass spectrometer. Repeated analyses of NBS987 Sr standard gave $^{87}Sr/^{86}Sr$ of 0.710258 ± 0.000026 (mean and external 2σ error of twelve measurements). The ^{87}Sr-^{86}Sr ratios are reported relative to $^{87}Sr/^{86}Sr$ = 0.71024 of NBS987 and the external error is estimated to be better than 0.002%. Repeated analyses of La Jolla Nd standard gave $^{143}Nd/^{144}Nd$ of 0.511849 ± 0.000011 (mean and external 2s error of eleven measurements); external error in the reported ^{143}Nd-^{144}Nd ratios is estimated to be better than 0.0025%.

4. Whole-rock geochemistry

4.1. General characteristics and grouping

The geochemical data for the dike samples show a wide range of major element contents (e.g., MgO = 5–28 wt. %, SiO_2 = 44–53 wt. %, CaO = 6–12 wt. %, Al_2O_3 = 6–14 wt. %, and Na_2O+K_2O = 1.0–3.7 wt. %; Table 1; Fig. 2). On the basis of CIPW norms, the rocks range from quartz- and olivine-tholeiites to mildly alkaline basalts. Following the guidelines of Le Bas (2000), samples with MgO < 12 wt. % are referred to as basalts or picrobasalts, samples with MgO = 12–18 wt. % are classified as picrites, and samples with MgO > 18 wt. % can be designated as meimechites. The high-MgO samples are characterized by exceptionally high FeO_{tot} contents (~11–17 wt. %) that distinguish them from MgO-rich Karoo lavas (Fig. 2a). Five picrite samples from three dikes have FeO_{tot} > 13 wt. % and are classified as ferropicrites. We emphasize that the meimechitic samples are geochemically quite similar to the ferropicrites (cf. Table 1) and notably different from alkaline meimechites from the type locality in Siberia ($SiO_2 \approx 40$ wt. %; $Al_2O_3 \approx 3$ wt. %; $Na_2O \approx 0.2$ wt. %; Fedorenko and Czamanske, 1997). The samples with MgO > 20 wt. % plot outside the area of Fig. 2; they contain abundant olivine phenocrysts (> 40 vol. %), have high Ni (> 1190 ppm), and are probably of accumulative origin. The FeO_{tot} contents of the basaltic samples show overlap with those of the CFB lavas of Vestfjella (Fig. 2a), but, similar to the meimechitic samples, they can be associated with the ferropicrites on the basis of their characteristic incompatible element signatures as discussed below.

Major, minor, and trace element contents are plotted against MgO in Fig. 2. We have used MgO as the differentiation index, because the relative Fe-enrichment of ferropicrites significantly lowers their Mg# [atomic $Mg/(Mg+Fe^{2+})$, assuming $Fe^{2+}/Fe_{tot} = 0.9$] relative to those of "common" basalts and picrites at a given MgO content (Fig. 2b). Analyses of several samples from individual dikes indicate that the chilled margins generally have lower MgO contents than the central parts (Table 1). Although the geochemical data show scatter at a given MgO content, some general trends can be seen: The concentrations of TiO_2, P_2O_5, V, and Nb generally increase and that of Cr decreases with decreasing MgO. Variation of Al_2O_3 records a possible inflection point at MgO ≈ 7 wt. %.

A subgroup of six samples can be distinguished based on relative enrichment of immobile high field strength elements (HFSE), e.g., P_2O_5 (0.37–0.42 wt. %), Nb (17–21 ppm), and TiO_2 (3.0–3.4 wt. %) (Fig. 2). They are further characterized by relative depletion in Cr (352–549 ppm) and V (258–319 ppm). These six samples are hereafter referred to as the enriched type to distinguish them from samples belonging to the depleted type; the latter is less enriched in most incompatible elements (e.g., TiO_2 = 1.5–2.9 wt. %, P_2O_5 = 0.17–0.25, and Nb = 6–9 ppm at MgO = 10–18 wt. %), but has exceptionally high V (300–448 ppm). One picrobasaltic dike (117-KHG-91) with MgO

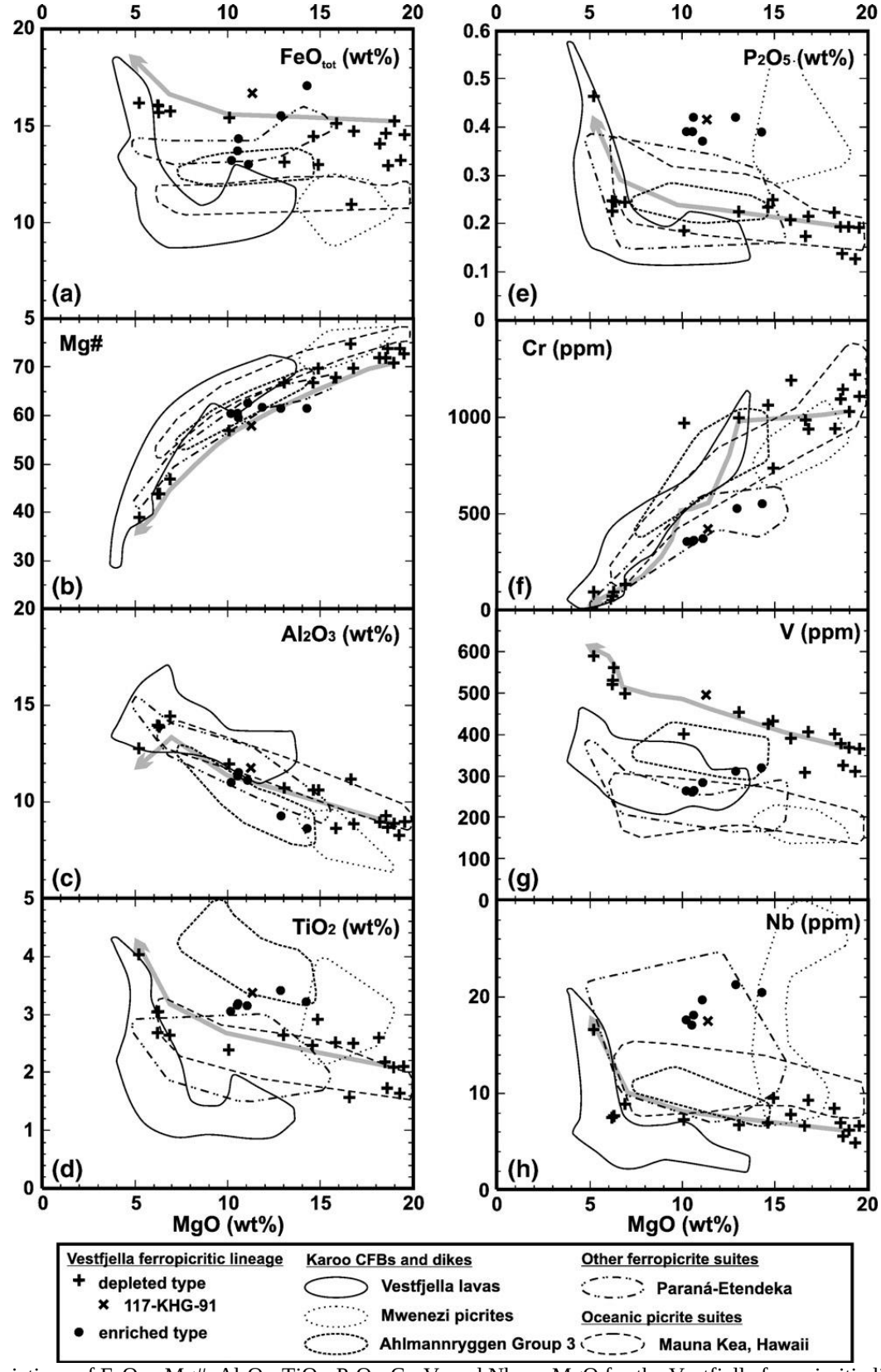

Fig. 2. Variations of FeO_{tot}, Mg#, Al_2O_3, TiO_2, P_2O_5, Cr, V, and Nb vs. MgO for the Vestfjella ferropicritic lineage. See Section 4.1. for the definition of the depleted and enriched type. Compositions of Vestfjella lavas (Luttinen et al.,1998; Luttinen and Furnes, 2000),Mwenezi picrites (Cox and Bristow,1984; Ellam and Cox,1989), Ahlmannryggen Group 3 dikes (Riley et al., 2005), Paraná–Etendeka ferropicritic rocks (Gibson et al., 2000), and Hawaiian lavas (Mauna Kea; Rhodes and Vollinger, 2004) are shown for comparison. Modeled liquid lines of descent (see Section 8. for parameters and discussion) of a melt corresponding to sample AL/WM1e-98 are shown as gray arrows. Mg#=atomic $Mg/(Mg+Fe^{2+})$; $Fe^{2+}/Fe_{tot}=0.9$.

= 11 wt. % has high incompatible element contents comparable with the enriched type (e.g., P_2O_5 = 0.41 wt. % and Nb = 17 ppm), but, based on its high V (487 ppm) and the overall geochemical signature (see below), we associate it with the depleted type.

4.2. Incompatible trace elements

The REE geochemistry of the ferropicritic lineage is characterized by enrichment in the light REE (LREE) with chondrite-normalized $(La/Yb)_N$ of 4–9 (Fig. 3). Most of the samples have small positive Eu-anomalies [$(Eu/Eu^*)_N$ = 1.0–1.2; $Eu^* = \sqrt{(Sm*Gd)_N}$]. The $(La/Sm)_N$ values of the enriched type (1.5–1.8) are higher than those of the depleted type (1.1–1.4). Both types have high $(Sm/Yb)_N$ and the enriched type has systematically higher values (4.9–5.4) than the depleted type (3.2–4.5). The anomalous depleted picrobasalt 117-KHG-91 bears resemblance to the enriched type due to high $(La/Sm)_N$ = 1.8 and $(Sm/Yb)_N$ = 5.0 values.

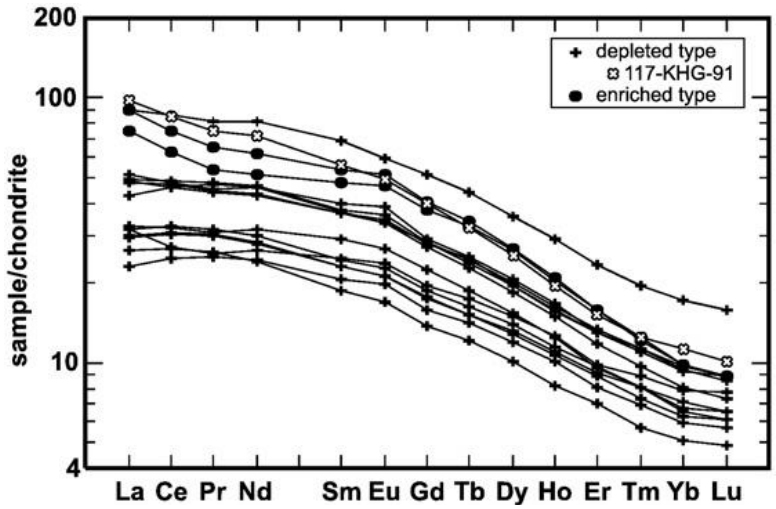

Fig. 3. Chondrite-normalized REE patterns for the Vestfjella ferropicritic lineage. Normalizing values are after McDonough and Sun (1995).

Primitive mantle-normalized incompatible element signatures confirm the division of the ferropicritic lineage into two different types (Fig. 4). The enriched type is characterized by a relatively smooth signature, whereas the depleted type records marked positive and negative anomalies. Generalizing, the enriched type shows enrichment from Th to Ta and depletion from Ta to Sc, with a small peak at V [$(V/Lu)_N$ = 1.0–1.3] and a trough at Zr and Hf. The smooth incompatible element signature with primitive mantle-like $(Nb/La)_N$ (0.9-1.0) combined with high $(Nb/Zr)_N$ (1.7–2.0) and $(Zr/Y)_N$ (2.2–2.4) indicates broad geochemical OIB-affinity for the enriched type (Fig. 4). The depleted type shows general enrichment from Th to Sr and depletion from Sr to Sc, with a trough at P and a pronounced peak at V with $(V/Lu)_N$ = 1.4–2.3. The incompatible element signature of the depleted ferropicrites shows notably similar general characteristics [e.g., $(Nb/Zr)_N$ = 0.9–1.1 and $(Zr/Y)_N$ = 2.6–2.7] to that of some Hawaiian picrites (Fig. 4). A review of published geochemical data using the GEOROC database (http://georoc.mpch-mainz.gwdg.de/georoc/) indicates, however, that the pronounced positive V anomaly and the negative P anomaly are quite uncommon in OIB, MORB and CFB lavas and dikes (cf. Fig 4), but common in ferropicrites (e.g., Hanski, 1992).

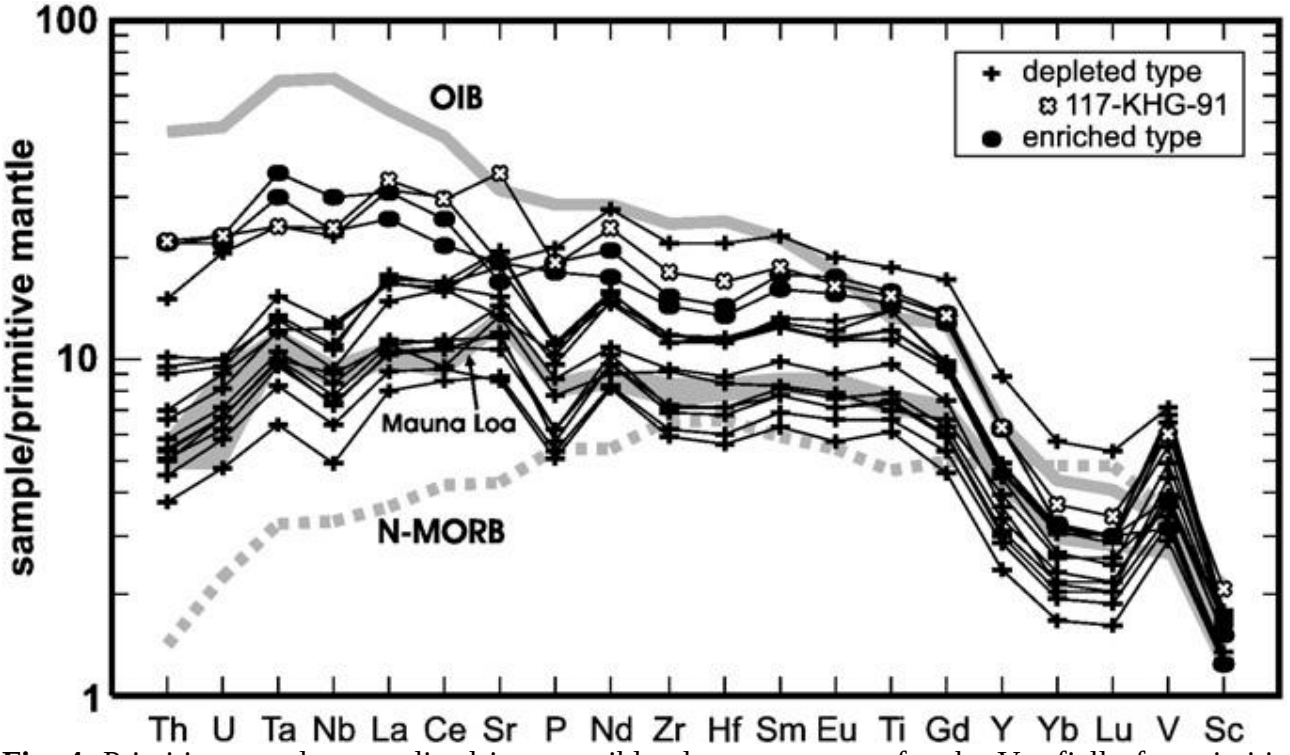

Fig. 4. Primitive mantle-normalized incompatible element patterns for the Vestfjella ferropicritic lineage. Average compositions of N-MORB (Sun and McDonough, 1989; V and Sc from Salters and Stracke, 2004), OIB (Sun and McDonough, 1989; V and Sc calculated after GEOROC (http://georoc.mpch–mainz.gwdg.de/georoc/)), and subset of Hawaiian picrites (Mauna Loa; Gaffney, 2002) are shown in gray for comparison. Normalizing values are after Sun and McDonough (1989) and, for V and Sc, after McDonough and Frey (1989).

5. Neodymium and strontium isotopes

Neodymium and strontium isotopic data on eight samples representing the ferropicritic lineage are shown in Table 2 and illustrated in Fig. 5. Isotopically, the studied dikes are markedly different from the majority of Karoo-related CFBs based on their radiogenic Nd initial isotopic ratios at 180 Ma. The depleted ferropicrites AL/B16-98 and AL/WM1e-98 show highly radiogenic initial Nd isotopic compositions with ε_{Nd} of +7.2 and +8.0, respectively. The ε_{Nd} values of the depleted basalts are somewhat lower and range from +6.3 to +4.8, and those of the enriched ferropicrites range from +3.6 to +1.8. The Sr isotopic compositions are coupled with Nd isotopic compositions and the initial ε_{Sr} values range from highly negative (–18.9 to –11.2) in the depleted ferropicrites and basalts to slightly positive (+0.2 to +10.6) in the enriched ferropicrites. Overall, the Nd and Sr isotopic compositions of the ferropicritic lineage plot within the depleted mantle array, overlap with the field of CT2 dikes of Vestfjella, and are comparable with those of ferropicrites and some other dikes belonging to Group 3 of Ahlmannryggen (Fig. 5). The depleted ferropicrites exhibit DM-model ages of ~180 Ma (De Paolo, 1981) consistent with derivation of their parental magmas from an old, highly LREE-depleted mantle source (Fig. 5).

In general, the Vestfjella ferropicrites plot within the isotopic compositional field of other Phanerozoic ferropicrites (Fig. 5b). Their isotopic compositions are in fact remarkably variable compared to individual ferropicrite suites with the depleted ferropicrites showing affinity to the ferropicrites of Japan, Ahlmannryggen, Madagascar, and Siberia and the enriched ferropicrites resembling the ferropicrites of Paraná-Etendeka (Fig. 5b). Compared to the depleted ferropicrites, the ferropicrites of Ahlmannryggen, Madagascar, and Siberia exhibit relatively high ε_{Sr} at given ε_{Nd}, however.

Heinonen, J.S., Luttinen, A.V., 2008. Jurassic dikes of Vestfjella, western Dronning Maud Land, Antarctica: geochemical tracing of ferropicrite sources. Lithos 105 (3–4), 347–364.
http://dx.doi.org/10.1016/j.lithos.2008.05.010 (Author's postprint)

Table 2
Isotopic data for the Vestfjella ferropicritic lineage

Sample	Mg#*	Rb†	Sr†	$^{87}Rb/^{86}Sr$	$^{87}Sr/^{86}Sr$‡	$^{87}Sr/^{86}Sr$ (i)§	ε_{Sr}§	Sm	Nd	$^{147}Sm/^{144}Nd$	$^{143}Nd/^{144}Nd$‡	$^{143}Nd/^{144}Nd$(i)§	ε_{Nd}§
Depleted type		(ppm)	(ppm)					(ppm)	(ppm)				
AL/WM1e-98	71	8.37	303	0.07992	0.703200 ± 50	0.703036	- 18.4	5.10	18.89	0.1633	0.513008 ± 10	0.512816	+ 8.0
AL/B16-98	69	6.84	321	0.06165	0.703118 ± 20	0.702996	- 18.9	6.11	23.51	0.1572	0.512958 ± 10	0.512773	+ 7.2
X6-KHG-90	46	3.20	479	0.01933	0.703550 ± 50	0.703507	- 11.2	5.27	20.83	0.1529	0.512861 ± 11	0.512681	+ 5.4
AL/KB5-98	44	4.63	395	0.03391	0.703482 ± 50	0.703397	- 12.7	5.68	22.17	0.1575	0.512848 ± 08	0.512662	+ 5.0
128-KHG-91	43	2.70	422	0.01851	0.703480 ± 50	0.703439	- 12.2	5.44	21.22	0.1550	0.512833 ± 14	0.512650	+ 4.8
X2-KHG-90	39	14.20	441	0.09315	0.703390 ± 50	0.703144	- 16.2	9.84	39.43	0.1509	0.512908 ± 11	0.512730	+ 6.3
Enriched type													
AL/B20a-98	62	11.61	355	0.09461	0.704550 ± 50	0.704320	+ 0.2	8.12	32.10	0.1531	0.512744 ± 13	0.512564	+ 3.1
AL/B7-98	60	7.85	415	0.05472	0.705180 ± 50	0.705044	+ 10.6	7.28	27.27	0.1615	0.512688 ± 12	0.512498	+ 1.8
14-KHG-90**	*62*	*11.05*	*374.9*	*0.08523*	*0.704563 ± 13*	*0.70434*	*+ 0.7*	*7.05*	*28.35*	*0.1503*	*0.512768 ± 10*	*0.512591*	*+ 3.6*

* Mg-number [atomic $Mg/(Mg+Fe^{2+})$; $Fe^{2+}/Fe_{tot} = 0.9$]
** Data from Luttinen et al. (1998).
† Analyzed with ICP-MS at the Washington State University (cf. Table 1).
‡ $^{87}Sr/^{86}Sr$ normalized to $^{86}Sr/^{84}Sr = 0.1194$ and $^{143}Nd/^{144}Nd$ normalized to $^{146}Nd/^{144}Nd = 0.7219$. Within-run error expressed as $2\sigma_m$ in the last significant digits.
§ Initial $^{87}Sr/^{86}Sr$, $^{143}Nd/^{144}Nd$, ε_{Sr}, and ε_{Nd}, calculated at 180 Ma using $^{87}Sr/^{86}Sr = 0.7045$ and $^{87}Rb/^{86}Sr = 0.0816$, and $^{143}Nd/^{144}Nd = 0.512638$ and $^{147}Sm/^{144}Nd = 0.1966$, respectively.

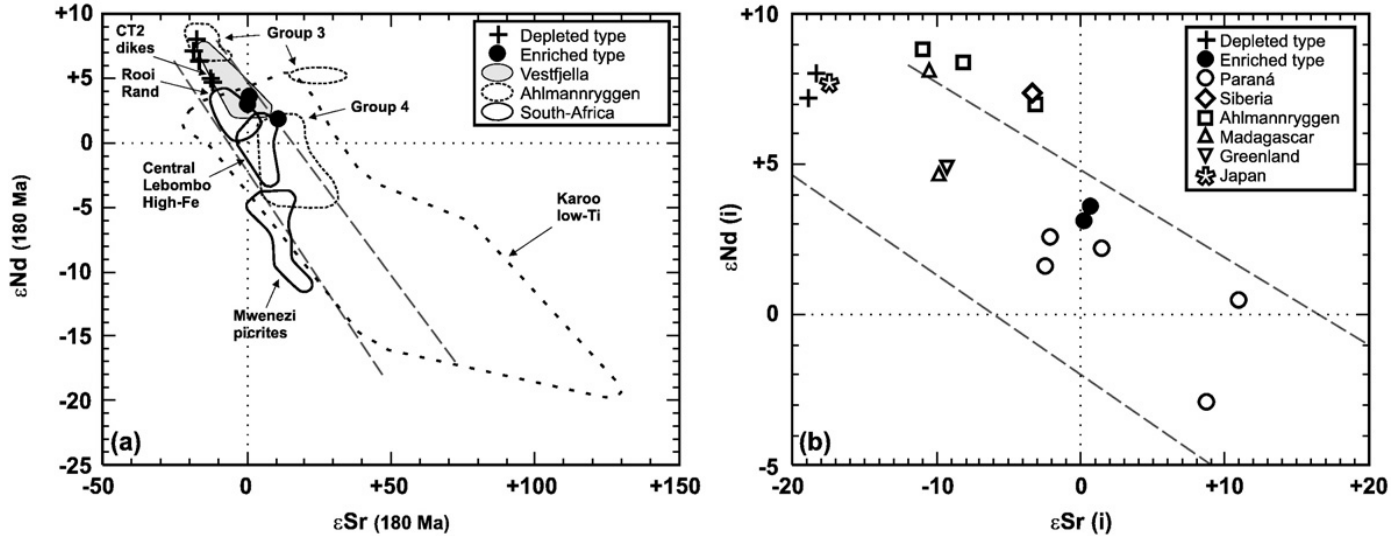

Fig. 5. ε_{Nd} vs. ε_{Sr} diagrams of the Vestfjella ferropicritic lineage and (a) other Karoo-related CFB suites and (b) Phanerozoic rocks reported as ferropicrites. The dashed lines indicate the oceanic mantle array and its low-ε_{Nd}–high-ε_{Sr} continuation (cf. Menzies and Murthy, 1980). Data sources in (a): Hawkesworth et al. (1984), Ellam and Cox (1991), Sweeney et al. (1994), Luttinen and Furnes (2000), Riley et al. (2005), and Jourdan et al. (2007a,b), Lightfoot et al. (1993), Fram and Lesher (1997), Storey et al. (1997), Gibson et al. (2000), Riley et al. (2005), and Ichiyama et al. (2006).

6. Petrography

6.1. Picritic and meimechitic samples

The picritic and meimechitic samples are olivine porphyritic and some of the picritic samples also contain clinopyroxene phenocrysts. The depleted and enriched types show similar petrographic characteristics, except that the samples representing the enriched type are more altered than the depleted type samples. Euhedral or subhedral olivine is the main phenocryst phase (13–49 vol. %; Ø ≤ 5 mm). It is commonly well-preserved in the depleted type samples, but invariably altered to mafic layer silicates in the enriched type samples. Representative data on olivine phenocrysts in two depleted ferropicrite dikes record relatively high CaO typical of volcanic olivine and Mg-rich compositions ($Fo_{79–88}$; Table 3). In the ferropicritic dike from Muren (sample AL/WM1e-98), some phenocrysts have a more magnesian rim relative to the core. Olivine phenocrysts in both geochemical types contain large, round inclusions (Ø ≤ 0.8 mm) that consist of clinopyroxene, kaersutitic hornblende, spinel, and fine-grained mesostasis. Kaersutite is found only in these inclusions. Clinopyroxene is found as phenocrysts and microphenocrysts (5–33 vol. %; Ø ≤ 1.5 mm) in picrites with MgO < 15 wt. %. It is subhedral, zoned, slightly reddish, often glomerophyric, and invariably fresh. Plagioclase has not been observed as a phenocryst phase in the picrites or meimechites.

The groundmass consists of fine- to medium-grained prismatic clinopyroxene, interstitial plagioclase, Fe-Ti oxides, and minor quantities of brownish mica, and secondary sericite, saussurite, and oxides. Some of the samples contain sparse amygdales: the vesicles (Ø < 1mm) are filled with secondary quartz and mafic layer silicates.

Table 3
Representative olivine compositions for the depleted ferropicrites of Vestfjella

Sample	AL/B16-98	AL/B16-98	AL/B16-98	AL/B16-98	AL/B16-98	AL/WM1e-98	AL/WM1e-98	AL/WM1e-98	AL/WM1e-98	AL/WM1e-98
crystal	1	2	2	3	3	1	2	2	3	3
position	core	core	rim	core	rim	core	core	rim	core	rim
SiO_2	39.92	40.10	39.81	39.76	39.63	40.28	39.20	39.88	38.91	39.43
TiO_2	0.00	0.04	0.02	0.01	0.00	0.06	0.00	0.04	0.01	0.04
Cr_2O_3	0.09	0.09	0.11	0.04	0.05	0.11	0.04	0.08	0.02	0.07
FeO	11.92	12.48	13.31	14.33	16.60	13.28	17.44	14.23	19.42	16.78
MnO	0.18	0.12	0.14	0.20	0.24	0.16	0.32	0.15	0.28	0.26
NiO	0.39	0.48	0.43	0.40	0.38	0.40	0.30	0.39	0.26	0.31
MgO	46.85	46.86	46.07	44.97	43.07	46.02	42.86	44.70	41.09	43.20
CaO	0.25	0.27	0.31	0.35	0.38	0.44	0.32	0.43	0.45	0.47
Na_2O	0.14	0.21	0.30	0.27	0.15	0.18	0.20	0.20	0.21	0.09
K_2O	0.01	0.01	0.03	0.03	0.00	0.00	0.00	0.00	0.01	0.02
Sum	99.75	100.67	100.54	100.37	100.51	100.93	100.67	100.08	100.67	100.68
Fo content	88	87	86	85	82	86	81	85	79	82

Data obtained by electron microprobe (Cameca SX-100) analysis at Department of Earth Sciences at University of Cambridge. The microprobe was operated at 20 kV accelerating voltage, 1 μm beam width, 3 nA beam current, and using energy dispersive X-ray detector.

6.2. Basaltic samples

The basaltic dikes typically are clinopyroxene or plagioclase porphyritic (9–20 vol. % of phenocrysts), but some of them show equigranular subophitic textures in the central parts. Clinopyroxene phenocrysts are confined to basaltic dikes with MgO > 7 wt. %, whereas plagioclase phenocrysts are only found in dikes with MgO < 7 wt. %. The main minerals in the equigranular rocks are plagioclase (38–60 vol. %), clinopyroxene (24–38 vol. %), oxides (5–10 vol. %), and

olivine (0–22 vol. %). Olivine phenocrysts are found only in basalts with MgO > 10 wt. % and are completely altered to mafic layer silicates in the enriched type samples. Clinopyroxene is invariably fresh, whereas plagioclase is commonly slightly altered to sericite and saussurite. Depleted picrobasalt 117-KHG-91 is characterized by abundant euhedral ilmenite and zoned clinopyroxene that shows purple to brownish pleochroism indicative of a high Ti content.

7. Assessing melt compositions: olivine–melt equilibrium

Accumulation of relatively Fe-rich olivine (e.g., Fo_{70}) from melts with relatively low Mg and Fe contents can generate ferropicritic whole-rock compositions. From a petrogenetic point of view it is crucial to evaluate whether the whole-rock data on the Vestfjella ferropicrites represent true Fe-rich melt compositions. We address this question by using compositional data on olivine in two depleted type dikes that show ferropicritic to meimechitic whole-rock compositions (Table 3).

The analyzed samples are characterized by primitive olivine (> Fo_{79}; Table 3). The most Mg-rich olivine compositions (Fo_{86} in AL/WM1e-98 and Fo_{88} in AL/B16-98) correspond to olivine that would crystallize from primary mantle-derived melts. Assuming a $K_D(Fe\text{-}Mg)^{ol\text{-}liq}$ of 0.35 [mean value for magmas equilibrated at elevated pressures (>2.3 GPa); Putirka, 2005], $Fo_{86\text{-}88}$ would have been in equilibrium with a melt with Mg# = 68–71, respectively (e.g., if MgO = 16 wt. %, then FeO_{tot} = 13–15 wt. %). Importantly, the ferropicritic (MgO = 15–17 wt. %) and also the meimechitic (MgO = 18–19 wt. %) parts of these dikes show Mg# within or very close to this range (Table 1). Some of the meimechitic samples with Mg# = 71–73 probably record olivine accumulation in picritic parental magma, however. Similarly, the highly magnesian (MgO > 23 wt. %) and olivine-rich (> 40 vol. %) samples from meimechitic boulders are likely to represent cumulates, although we do not have olivine data for them. These calculations and observations indicate that the depleted ferropicrites are likely to represent true ferropicritic melts. The similar FeO_{tot} contents of the ferropicritic and meimechitic samples underpin the fact that accumulation of Mg-rich olivine phenocrysts does not lead to Fe-enrichment in the cumulate.

We cannot similarly evaluate whether the more altered enriched type samples represent melt compositions. Nonetheless, the chilled margin sample AL/B20a-98 geochemically (MgO = 12.84 wt. %, FeO_{tot} = 15.50 wt. %) and petrographically resembles the depleted type chilled margins, and may well represent a ferropicritic melt composition. The possibility that the exceptionally high Fe contents of some of the enriched type samples are caused by accumulation of Fe-rich olivine cannot be completely excluded, however.

8. Geochemical effects of alteration and differentiation: tracing primary melt signatures

Petrogenetic studies on the ferropicritic lineage require evaluation of the effects of magmatic differentiation and subsequent secondary alteration processes on the primary geochemical signatures inherited from the mantle source.

Pseudomorphed olivine, sericitized plagioclase, and amygdales indicate subsolidus alteration of the studied samples. Most of the samples, however, are relatively well-preserved compared to the CFBs they intrude. HFSEs show systematic behavior in all samples (Fig. 4); they are widely regarded as immobile elements and probably have not been affected by subsolidus processes. In contrast, the large ion lithophile elements (LILE), such as Rb and Ba, show relatively large variations (Table 1). The least-altered samples have uniform LILE/HFSE values that may reflect magmatic compositions, but we have excluded LILE from the discussion due to obvious uncertainties related to these easily mobilized elements.

The wide range of MgO contents (5.1–27.5 wt. %) and the high amount of phenocrysts indicate that fractional crystallization had a significant role in the evolution of the ferropicritic lineage. We have modeled fractional crystallization of a depleted ferropicrite parental melt at

different pressure conditions using the PELE software (Boudreau, 1999). Full listings of the models are available from the first author upon request. Fractional crystallization models using a parental melt corresponding to sample AL/WM1b-98 yielded best results when cooling was coupled with decompression from 2.5 GPa and 1580 ºC (liquidus T at 2.5 GPa) to 0.1 GPa and 1100 ºC. The simulated liquid line of descent and the composition of the solid fractionate fit fairly well with the geochemical data and the phenocrysts assemblages of the ferropicritic lineage (Fig. 2). Specifically, crystallization of clinopyroxene before plagioclase at >10 wt. % MgO, as indicated by the geochemical and petrographical data, was successfully simulated only at relatively high pressures (> 1 GPa). A polybaric crystallization model is further compatible with the reverse zoning observed in olivine phenocrysts (Table 3) as pressure correlates positively with the Fe-Mg olivine-liquid K_d (Ulmer, 1989). In the best-fit model, the crystallization sequence of fractionating minerals was olivine (liquidus phase), Cr-spinel (MgO < 13 wt. %), clinopyroxene (MgO < 11 wt. %), and plagioclase (MgO < 7 wt. %). Such a fractionation model will not significantly change the incompatible element ratios of magmas, apart from those involving Sr in the most evolved depleted type samples (MgO < 7 wt. %), which is accordant with the conformable mantle-normalized patterns of depleted type samples in Fig. 4.

Most of the Karoo-related lavas and dikes show strong geochemical indications of contamination with crust or lithospheric mantle (e.g., Ellam and Cox, 1991; Sweeney et al., 1991; Luttinen et al., 1998; Jourdan et al., 2007a) and the ferropicritic magmas most probably have also interacted with the lithosphere. We have used contamination-sensitive trace element ratios (Th/Ta, La/Sm, Ti/Zr, and La/Nb) and ε_{Nd} values to evaluate whether the incompatible element and isotopic signatures of the ferropicritic lineage have been significantly overprinted by contamination. The results of EC-AFC modeling (Bohrson and Spera, 2001) of crustal contamination and AFC modeling (DePaolo, 1981) of lithospheric mantle contamination are summarized in Fig. 6 and the model parameters are listed in Table 4. In the case of lithospheric mantle contamination, we preferred simple AFC modeling (cf. Ellam and Cox, 1991; Luttinen and Furnes, 2000) due to uncertainties regarding partial melting and dissolution processes (Foley, 1992) and the composition and thermodynamic properties of metasomatized lithospheric mantle. For the lithospheric mantle-derived and crustal contaminants we used, respectively, a Vestfjella lamproite (Luttinen et al., 2002) and hypothetical Archean and Proterozoic granitoids in accordance with the proximity of Vestfjella to the Archean-Proterozoic lithospheric boundary of DML (Fig. 1b).

The depleted ferropicrite AL/WM1e-98 has markedly high initial ε_{Nd} (+8.0) corresponding to the depleted mantle of DePaolo (1981), clearly has not been extensively contaminated by lithospheric material, and has thus been selected to represent the composition of the parental melt. We have evaluated the following scenarios: (1) The depleted basalts represent contaminated differentiates of the depleted ferropicrites, (2) the enriched ferropicrites represent contaminated differentiates of the depleted ferropicrites, and (3) the ferropicritic lineage represents contaminated differentiates of Group 3 magmas from Ahlmannryggen (Riley et al., 2005) that record the highest initial ε_{Nd} values so far measured for Karoo LIP (up to +9.0). Although the compositions of lithospheric contaminants are hypothetical, we believe that the results illustrate the potential of contamination processes to overprinting primary magmas and can be used for estimating the geochemical effects of contamination on the ferropicritic lineage.

Qualitatively, our models illustrate the controlling influence of lithospheric contamination on the geochemical signatures of many Karoo-related magma types, e.g., Vestfjella CFBs, Ahlmannryggen Group 4 dikes, and the Mwenezi picrites (Fig. 6). In the case of the ferropicritic lineage, the key results of the models can be summarized as follows: (1) Depleted basalts with relatively low ε_{Nd} values ($\leq$ +6.3) may have been contaminated with small amounts (< 2 %) of lithospheric material (Fig. 6), but the overall geochemical effect of lithospheric overprinting is undetectable in the mantle-normalized signature (cf. Fig. 4). (2) Based on La/Sm, Th/Ta, and ε_{Nd}, the enriched type samples could record incorporation of ~2% of lithospheric mantle material into

depleted ferropicrite parental magma (Fig. 6a, c). The combination of high Ti/Zr and low La/Nb values in the enriched type, however, implies that their geochemical signature is not caused by contamination of any presently known Karoo magma type (Fig. 6b). The relatively low ε_{Nd} values (+3.6 to +1.8) of the enriched type are comparable to those of Hawaiian tholeiites and compatible with derivation of the enriched type from a slightly LREE-enriched mantle source relative to DM (Fig. 6c, d). Minor overprinting of the geochemical and isotopic signatures, however, cannot be precluded. (3) The Vestfjella ferropicrites and Group 3 dikes (including ferropicrites) from Ahlmannryggen are unlikely to represent co-genetic magmas despite the fact that some of their geochemical differences could be explained by similar contamination models using a Group 3 picrite with $\varepsilon_{Nd} > +8$ as a parent magma (Fig. 6a, c, d): Fractional crystallization and contamination processes typically lead to increasing Zr and heavy REE concentrations and decreasing Ti/Zr values in the daughter magmas. The systematically higher Zr (>228 ppm) and Lu (>0.36 ppm), and lower Ti/Zr (< 110; Fig. 6b) of Group 3 picrites (Riley et al., 2005) make them implausible parental magmas of the Vestfjella ferropicrites (cf. Table 1).

Table 4
Thermal and compositional parameters for the contamination models

EC-AFC model parameters				
Magma liquidus temperature				1510 ºC
Magma initial temperature				1510 ºC
Assimilant liquidus temperature				1000 ºC
Assimilant initial temperature				600 ºC
Solidus temperature				900 ºC
Equilibration temperature				950 ºC
Isobaric specific heat of magma				1484 J/kg K
Fusion enthalpy				270000 J/kg
Isobaric specific heat of assimilant				1370 J/kg K
Crystallization enthalpy				396000 J/kg
AFC model parameters				
Rate of assimilation				0.5
Compositional parameters*:				
	parent:	*contaminants:*		
	ferropicrite	Archean	Proterozoic	lamproite
Th	0.49 *(0.001)*	3.0 *(0.04)*	10.7 *(0.04)*	26.1 *(0.04)*
Ta	0.43 *(0.29)*	0.6 *(0.13)*	0.9 *(0.14)*	14.6 *(0.09)*
La	7.75 *(0.017)*	13.81 *(0.17)*	30 *(0.22)*	278 *(0.12)*
Nd	14.51 *(0.04)*	11.42 *(0.14)*	26 *(0.17)*	229 *(0.078)*
Sm	4.32 *(0.11)*	1.8 *(0.13)*	4.5 *(0.15)*	36.4 *(0.088)*
Ti	12420 *(0.078)*	1320 *(0.51)*	3000 *(0.51)*	23880 *(1.57)*
Zr	104 *(0.094)*	131 *(0.15)*	190 *(0.18)*	1076 *(0.18)*
Nb	6.05 *(0.088)*	7 *(0.5)*	25 *(0.59)*	170 *(0.072)*
ε_{Nd} †	+8	-52	-7	-6

* Element concentrations given in ppm. Numbers in parentheses indicate the bulk K_D values used in the model (compiled from http://www.earthref.org). Compositions of hypothetical ferropicrite primary magma (AL/WM1e-98; Table 1), Archean crustal contaminant (3.27 Ga Anhalt Granitoid Suite trondhjemite; average of eight samples from Hunter et al., 1992; Th and Ta from Rudnick and Fountain, 1995; ε_{Nd} from Luttinen and Furnes, 2000), Proterozoic crustal contaminant (Rudnick and Fountain, 1995; Ta from Rudnick and Gao, 2003; ε_{Nd} compatible with Maud Belt data of Arndt et al., 1991), and lithospheric mantle contaminant (lamproite AL/KB8-98 from Luttinen et al., 2002) shown.
† Calculated at 180 Ma (cf. Table 2)

In summary, the geochemical signatures (Fig. 4), and particularly the immobile incompatible element ratios of the ferropicritic lineage closely correspond to magmatic compositions and have not been significantly affected by alteration. Furthermore, fractional crystallization and lithospheric mantle contamination have not notably overprinted the geochemical signature of the depleted ferropicrites. We suggest that the geochemical signatures of the depleted ferropicrites, and possibly

also those of the enriched ferropicrites, record characteristic features of primary melts and can be regarded as geochemical tracers of mantle source regions. The basaltic and meimechitic differentiates of ferropicritic magmas are excluded from the petrogenetic discussion unless otherwise mentioned.

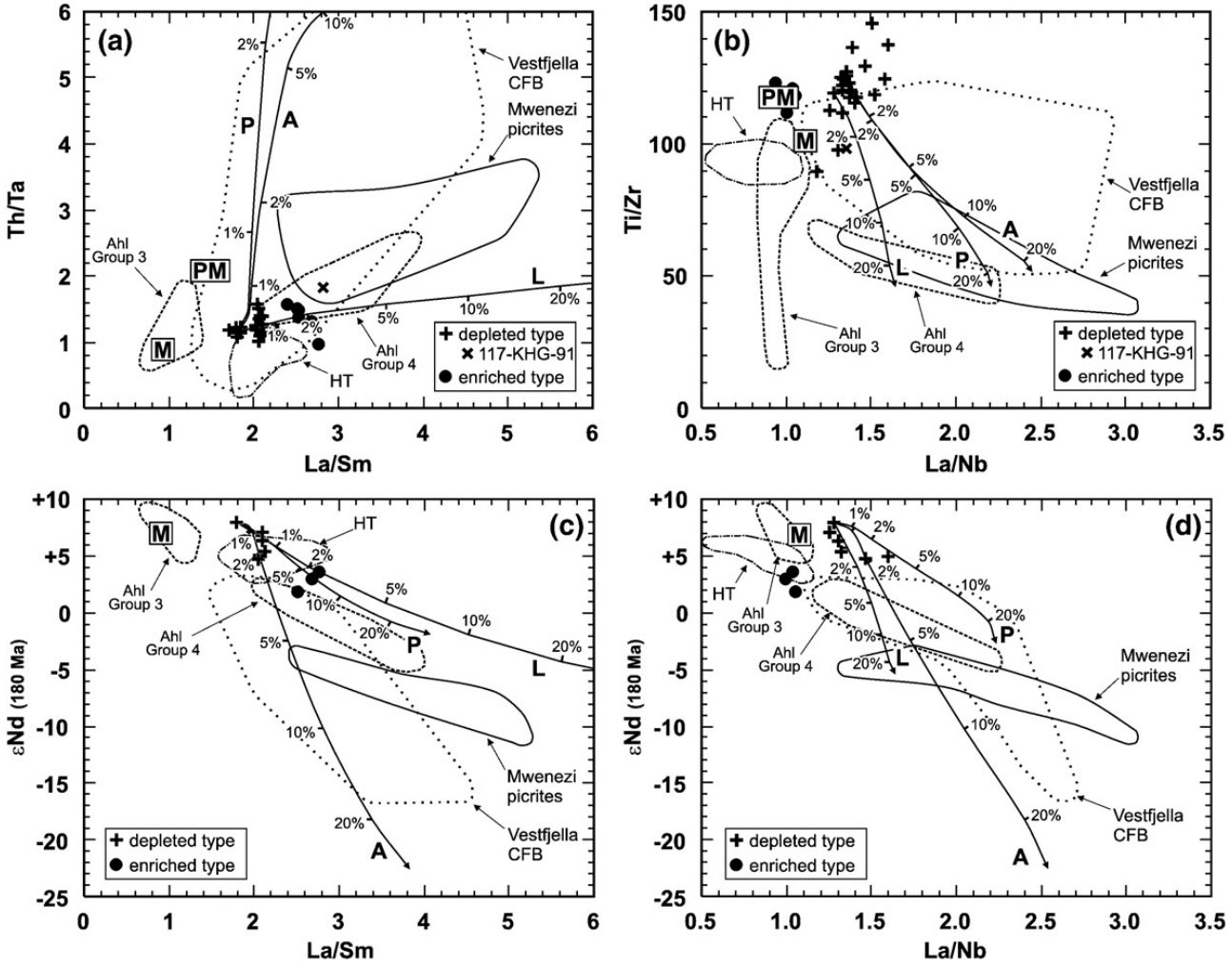

Fig. 6. Variations of (a) Th/Ta vs. La/Sm, (b) Ti/Zr vs. La/Nb, (c) ε_{Nd} (180 Ma) vs. La/Sm, and (d) ε_{Nd} (180 Ma) vs. La/Nb for the Vestfjella ferropicritic lineage. Compositions of Vestfjella lavas (Luttinen et al., 1998; Luttinen and Furnes, 2000), Group 3 and Group 4 dikes of Ahlmannryggen (Ahl; Riley et al., 2005), Mwenezi picrites (Ellam and Cox, 1989, 1991), Hawaiian tholeiites (HT; n≈50–250; data from GEOROC: http://georoc.mpch-mainz.gwdg.de/georoc/), primitive mantle (PM; Sun and McDonough,1989), and a MORB-like hypothetical parent of Vestfjella lavas (M; Luttinen et al., 1998) shown for comparison. Results of EC-AFC [with Archean crust (A) and Proterozoic crust (P) as end-members] and AFC [with lithospheric mantle (L) as an end-member] modeling of a hypothetical primary ferropicrite melt corresponding to sample AL/WM1e-98 also shown (see Table 4 for model parameters). Tick marks indicate the amount of assimilated material relative to the original primary melt.

9. Petrogenesis of the Vestfjella ferropicrites

The Vestfjella ferropicrites have significant geochemical affinities to rock types derived from hotspot-type mantle sources (Fig. 4). Geochemical data from oceanic islands worldwide indicate a significant component of subducted oceanic crust (eclogite) in hotspot mantle (e.g., Hofmann and White, 1982; Weaver, 1991; Sobolev et al., 2007). According to a popular theory, partial melting of relatively fusible eclogite inclusions produces SiO_2-rich melts that react with olivine in the host garnet peridotite and generate a secondary garnet pyroxenite source in upwelling mantle (Yaxley and Green, 1998; Sobolev et al., 2005). Subsequent melting of this "refertilized" source yields

parental melts with varying proportions of pyroxenite- and peridotite-derived components (Sobolev et al., 2005; 2007). Recent studies have concluded that some of the Hawaiian lavas lack the peridotite-derived component and represent partial melts of pyroxenite only (Herzberg, 2006). Recognizing the overall geochemical similarity of ferropicrites and OIBs and that the exceptionally high Fe and Ti contents of ferropicrites preclude a common peridotitic mantle source (Hanski, 1992), Gibson (2002) applied the "refertilized" source model to ferropicrite magmatism. Such a garnet-pyroxenite source is further supported by melting experiments on ferropicritic starting material (Tuff et al., 2005).

The Vestfjella ferropicrites include samples that probably represent near-primary melts. In the CMAS system of O'Hara (1968), these samples show affinity to melt compositions derived from mixed eclogite-peridotite source and garnet pyroxenite sources, but they also plot close to the field of garnet peridotite derived melts (Fig. 7a). Garnet peridotite-derived melts are highly magnesian (MgO > 20 wt. %), however, and notably low in FeO_{tot} and TiO_2, whereas the partial melts of garnet pyroxenites are similar to the Vestfjella ferropicrites (Fig. 7b). Given that both ferropicrites and oceanic island magma suites are probably generated from pyroxenite-bearing "refertilized" sources and that some OIPs represent melting of pyroxenite only, the systematically lower FeO_{tot} level in OIPs (~10–12 wt. %; Fig. 2) raises the question as to whether the generation of ferropicritic liquids requires specific melting conditions or exceptionally Fe-rich pyroxenite composition, or both.

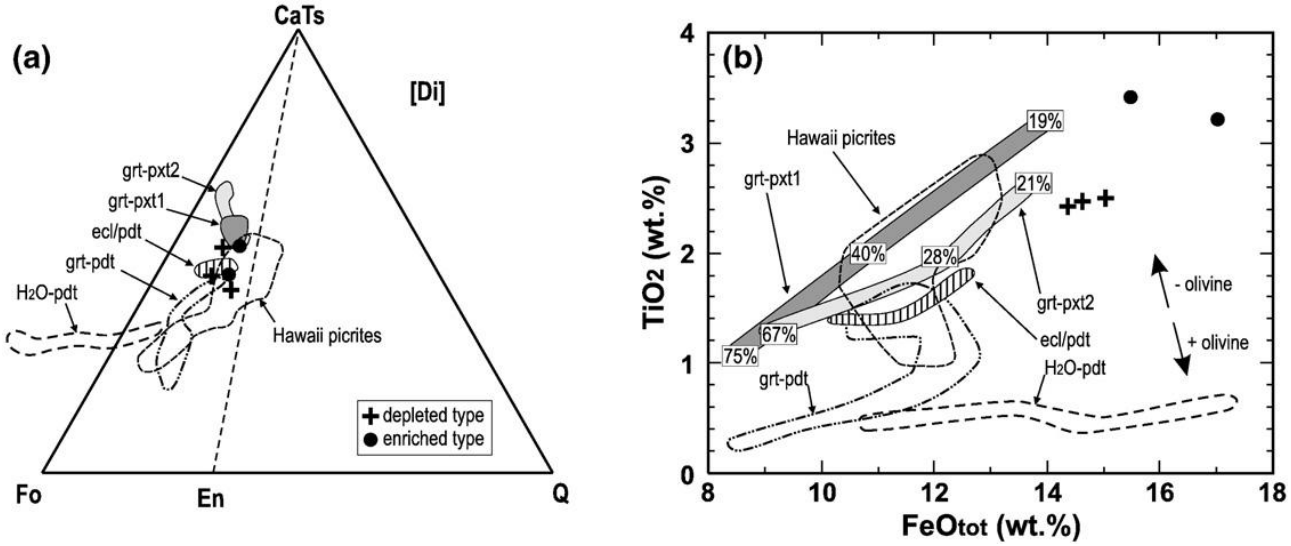

Fig. 7. Vestfjella ferropicrites compared with experimental peridotite- and pyroxenite-derived partial melts in equilibrium with garnet in (a) pseudoternary Fo-CaTs-Qz diagram (Di projection after Kogiso et al., 2003; using the method of O'Hara,1968) and (b) TiO2 vs. FeOtot diagram. Compositions of Hawaiian picrites (nN40; data from GEOROC: http://georoc.mpchmainz.gwdg.de/georoc/) are shown for comparison. Starting materials and data sources: grt-pxt1=Garnet-pyroxenite at 5 GPa (Kogiso et al., 2003), grt-pxt2=Garnet-pyroxenite at 2.5 GPa (Hirschmann et al., 2003), ecl/pdt=Eclogite-peridotite mixture at 3.5GPa (Yaxley andGreen,1998), grt-pdt=Garnet peridotite at 4–7GPa (Walter,1998),H2O-pdt=H2O-saturated peridotite at 5–11 GPa (Kawamoto and Holloway, 1997). Degree of melting in pyroxenite experiments is indicated in (b).

The influence of oxygen fugacity and water activity on the geochemical compositions of garnet pyroxenite-derived melts has not been experimentally studied. Judging from the OIB-like Fe_2O_3/FeO ratios (~0.1) of the Paraná-Etendeka ferropicrites (Gibson, 2002), however, generation of ferropicrites does not require exceptionally high fO_2 conditions during magma generation (cf. Francis et al., 1999). Also the significance of water for the petrogenesis of ferropicrites is poorly understood. Above all, opinions differ as to whether the parental melts have been hydrous (Hanski, 1992; Stone et al., 1997) or anhydrous (Gibson, 2002). The primary magmatic kaersutite in the olivine-hosted inclusions of the Vestfjella ferropicrites provides evidence for hydrous parental

magmas with up to ~2 wt. % of H_2O (cf. Stone et al., 1997). Nevertheless, based on the tendency of hydrous rock types to produce relatively Fe-poorer partial melts than corresponding dry rock types (e.g., Hirose and Kawamoto, 1995; Kawamoto and Holloway, 1997), the high Fe of the ferropicrite parental melts are not likely to result from high volatile contents in the mantle source (cf. Hanski, 1992; Gibson, 2002).

An increase in pressure and a decrease in the degree of partial melting increase the Fe contents of pyroxenite-derived liquids (Fig. 7b; cf. Hirschmann et al., 2003). The REE geochemistry of volcanic rocks has been frequently used for monitoring partial melting processes, i.e. the degree of melting and the pressure conditions (e.g., Putirka, 1999), although the interpretation is not straightforward due to several unknown melting parameters (e.g., source composition, residual assemblages, partition coefficients, nature of equilibrium). In general, however, variations of LREE/MREE and MREE/HREE are thought to be sensitive, respectively, to the degree and depth of melting (e.g., Tegner et al., 1998). The Vestfjella ferropicrites exhibit a strong garnet signature with high $(Sm/Yb)_N$ values (4.5–5.4) exceeding that of OIPs in general (cf. GEOROC; http://georoc.mpch-mainz.gwdg.de/georoc/). This could reflect magma generation at notably high pressures, but possible involvement of compositionally unusual sources cannot be excluded; in fact, the spiked geochemical signature strongly suggests a distinctive source for the depleted ferropicrites (Fig. 4).

Ichiyama et al. (2006) have suggested that suitable ferropicrite sources include recycled ferrobasalts and Fe-Ti gabbros. The amount of FeO_{tot} in such rock types may exceed 20 wt. % and is notably higher than in MOR basalts and gabbros in general (<12 wt. %). The geochemical signatures of ferrobasalts and Fe-Ti gabbros are quite different, however: The signatures of gabbroic rocks are sensitive to accumulation processes and separation of crystals and interstitial liquids in the solidification zones of axial magma chambers (cf. Sinton and Detrick, 1992). The effects of cumulus plagioclase (Ba, Sr, Eu), pyroxene (V), and Fe-Ti oxides (Ti, V) are readily predicted by mineral-melt K_D data (e.g., EarthRef: http://www.earthref.org/) and verified by trace element data on oceanic gabbros (e.g., Zimmer et al., 1995; Coogan et al., 2001) that frequently exhibit cumulate signatures (Fig. 8). The cumulate signature may be preserved to sub-arc depths during subduction (Becker et al., 2000; Spandler et al., 2004) and a cumulate source component may be traced by the diagnostic geochemical anomalies in mantle-derived melts (Sobolev et al., 2000; Yaxley and Sobolev, 2007).

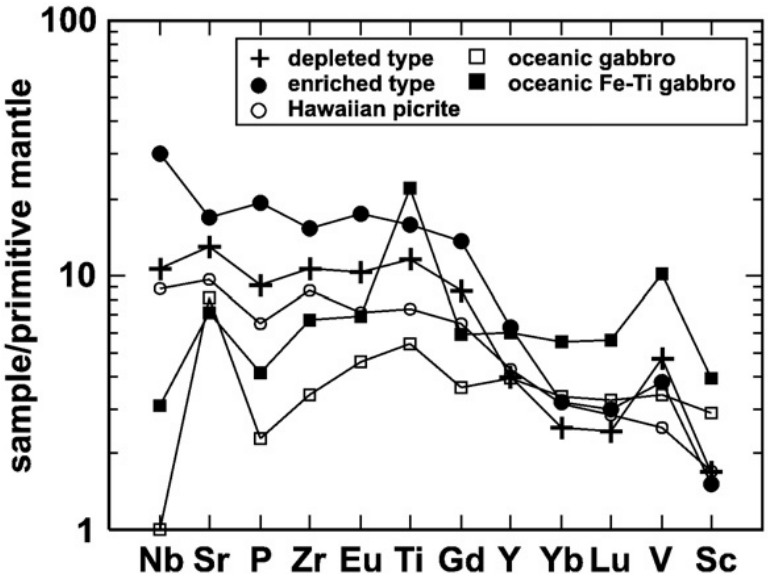

Fig. 8. Comparison of Vestfjella ferropicrites, pyroxenite-derived Hawaiian picrite (MLKAH-2 from Mauna Loa; Norman and Garcia, 1999; cf. Herzberg, 2006), and oceanic gabbros (averages of Coogan et al., 2001) using primitive mantle-normalized immobile incompatible element patterns. Normalizing values as in Fig. 4.

The geochemical signature of the enriched ferropicrites of Vestfjella resembles that of OIB (Fig. 4), whereas the depleted ferropicrites show marked similarities to oceanic gabbros, and Fe-Ti gabbros in particular (Fig. 8). We pay special attention to anomalous high $(V/Lu)_N$ values, which are extremely rare in intraplate and MOR basalts, but characterize the depleted ferropicrites as well as many oceanic gabbros. Theoretically, cumulus pyroxene can account for positive V anomalies in gabbroic rocks. Geochemical data on oceanic gabbros, however, show strong coupling of $(Ti/Gd)_N$ and $(V/Lu)_N$ (Fig. 8; cf. Coogan et al., 2001) suggesting that $(V/Lu)_N$ can be used as a geochemical tracer of cumulus Fe-Ti oxide in the source of pyroxenite-derived melts.

We have modeled partial melting of pyroxenite sources at high pressures using basaltic and gabbroic compositions for the eclogite component. In general, geochemical modeling cannot provide unique solutions due to many alternative melting scenarios and poorly constrained parameters. We tested the potential of pyroxenite sources with different eclogite compositions to produce partial melts with "common" OIP-type and ferropicrite-type geochemical signatures. The details of the model are listed in the caption of Fig. 9. Our models focus on REE characteristics and $(V/Lu)_N$ values and use modal melting models for eclogite and pyroxenite sources at high pressures (cf. Hirschmann et al., 2003; Kogiso et al., 2003; Yaxley and Sobolev, 2007).

Our results illustrate the potential of basalt-bearing and Fe-Ti gabbro-bearing sources to replicate some of the key geochemical differences between the Vestfjella ferropicrites and OIPs. The basalt-bearing source produces melting curves that coincide fairly well with the OIP field with respect to $(La/Sm)_N$, $(Sm/Yb)_N$, and $(V/Lu)_N$ at both modeled pressures, although the $(La/Sm)_N$ and $(V/Lu)_N$ values tend to be somewhat low at given $(Sm/Yb)_N$ (Fig. 9). In contrast, the depleted ferropicrites of Vestfjella plot close to the ~30 % partial melts of the Fe-Ti gabbro-bearing source at 5 GPa. The exceptionally Fe-rich (FeO_{tot} = 16.59 wt. %) depleted picrobasalt 117-KHG with anomalously high $(Sm/Yb)_N$ and $(La/Sm)_N$ compared to depleted ferropicrites and basalts (Fig. 9) could represent relatively lower degree of partial melting of the Fe-Ti gabbro-bearing source. We emphasize that the model parameters have been adopted directly from experimental studies and the compositional data for the different components represent averages or typical values; a better fit could be obtained by adjusting these parameters.

The enriched ferropicrites lack a strong cumulate signature and show an affinity to OIPs with respect to $(V/Lu)_N$. Considering that the Fe-Ti gabbro-bearing and the basalt-bearing sources produce rather similar melt compositions at 2.5 GPa due to retention of V by pyroxene-dominated residual assemblages (cf. Hirschmann et al., 2003), we consider two alternative interpretations to their geochemical characteristics: (1) The enriched ferropicrites record weakening of the Fe-Ti gabbro signature at relatively low pressure, or (2) the eclogite source component of the enriched ferropicrites was basalt-dominated and the magmas were generated by relatively low-degree melting at unusually high pressure (>5 GPa). Several pieces of evidence favor the latter scenario: First, the overall geochemical differences between the enriched and depleted ferropicrites point to different sources. Second, the higher Fe contents of the enriched ferropicrites are not compatible with derivation of these rocks from Fe-Ti gabbro-bearing source at lower pressure due to positive correlation of Fe-contents of partial melts and pressure. Third, the REE-characteristics are incompatible with relatively lower pressure of melting for the enriched ferropicrites. We speculate that the source of the enriched ferropicrites may have included a ferrobasalt component (cf. Byerly et al., 1976). Such a fertile eclogitic source component cannot be traced using $(V/Lu)_N$ and could have facilitated melting at unusually high pressure.

In conclusion, the geochemical compositions of the Vestfjella ferropicrites are compatible with derivation of these magmas from garnet pyroxenite sources. The geochemical signatures of the depleted and enriched ferropicrites probably manifest the combined influence of two key factors that facilitated generation of ferropicritic rather than OIP-type melts: (1) an unusually Fe-rich eclogite component and (2) low-degree partial melting at high pressures. The eclogite component in the depleted ferropicrites probably was Fe-Ti gabbro. Such a recycled cumulate source component,

primarily indicated by the anomalous $(V/Lu)_N$ values (Fig. 9), is likely to have high $(Sm/Nd)_N$ and low $(P/Nd)_N$ values (cf. Coogan et al., 2001) and would be expected to develop highly radiogenic Nd isotopic ratios and could help to explain the combination of high ε_{Nd} values and negative P anomalies typical of the depleted ferropicrites (Figs. 4, 5 and 8). The relatively small positive Ti anomaly of the depleted ferropicrites compared to that of Fe-Ti gabbro (Fig. 8) probably indicates retention of Ti by residual rutile or Ti-rich garnet during partial melting at great depths (Klemme et al., 2005; Zhang et al, 2003a). In the enriched ferropicrites, the eclogite component may have been ferrobasalt. An enriched basaltic source component is compatible with the lower ε_{Nd} values and the lack of cumulate signatures in these ferropicrites (Figs. 4, 5, 8 and 9).

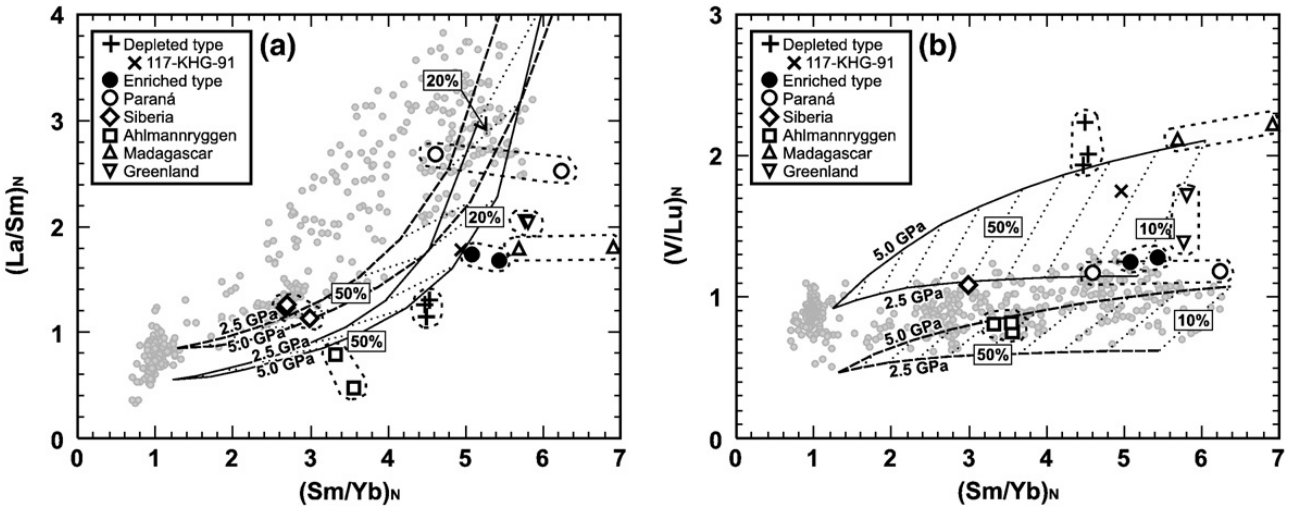

Fig. 9. Partial melting model of Phanerozoic ferropicrites (cf. Table 5), sample 117-KHG-91, and oceanic island picrites (grey spots) in (a) $(La/Sm)_N$ vs. $(Sm/Yb)_N$ and (b) $(V/Lu)_N$ vs. $(Sm/Yb)_N$ diagrams. Partial melt compositions of two hypothetical mantle pyroxenites are indicated at 2.5 GPa and 5.0 GPa. The peridotite component is pyrolite (McDonough and Sun, 1995) and the eclogite components correspond to average MORB (dashed lines; Salters and Stracke, 2004) and oceanic Fe–Ti gabbro (solid lines; Coogan et al., 2001). Partial melting of eclogite was modeled assuming 50% modal batch melting with cpx/grt=9:1 (cf. Yaxley and Sobolev, 2007) and partition coefficients of Halliday et al. (1995), Zack et al. (1997), and van Westrenen et al. (1999). Partial melting of the secondary pyroxenite (eclogite/peridotite=1:2; Sobolev et al., 2007) was modeled assuming modal batch melting with source modes corresponding to 2.5 GPa (cpx/grt=3:2, Hirschmann et al., 2003) and 5.0=GPa (cpx/grt=2:3, Kogiso et al., 2003) conditions using partition coefficient of Johnson (1994), Hauri et al. (1994), and Zack et al. (1997). Stippled lines and associated percentages indicate degree of melting. La, Sm, Yb normalized to C1-chondrite (McDonough and Sun, 1995), V and Lu normalized to primitive mantle (McDonough and Frey, 1989; Sun and McDonough, 1989; respectively). Data sources for ferropicrites given in Section 10.1. Oceanic island picrites (nN450) compiled from GEOROC: (http://georoc.mpch-mainz.gwdg.de/georoc/).

10. Fundamental ferropicrite factors: evidence from global dataset

To evaluate the general applicability of our petrogenetic model for the Vestfjella ferropicrites, we have compiled geochemical data on other ferropicritic suites. Our analysis is restricted to Phanerozoic rocks, which have developed under largely similar mantle conditions in terms of dynamics and temperatures.

10.1. Global ferropicrite dataset

Phanerozoic lavas and dikes of ferropicritic composition have been described from several CFB provinces including Paraná-Etendeka (Gibson et al., 2000), East Greenland (Fram and Lesher, 1997), Siberian Traps (Lightfoot et al., 1993; Wooden et al., 1993), Madagascar (Storey et al., 1997), and Karoo (Riley et al., 2005). Permian dikes from an accreted oceanic plateau in Japan (Mino-Tamba belt; Ichiyama et al., 2006) have also been described as ferropicrites, but these

samples are more accurately classified as meimechites (cf. Le Bas, 2000). Petrogenetic discussion on ferropicrites is complicated by the inconsistent classification criteria used by different authors: specifically, the diagnostic FeO_{tot} content of ferropicrites has varied from > 14 wt. % (Hanski and Smolkin, 1989) to > 12 wt. % (Riley et al., 2005). Given that FeO_{tot} of 12–13 wt. % are fairly common in intraplate picrites, we have defined ferropicrites as mildly alkaline or subalkaline picrites (Le Bas, 2000) with FeO_{tot} > 13 wt. % (cf. Gibson et al., 2000). This classification scheme is not regarded to represent a natural petrological division, but it helps us to identify possible key characteristics of exceptionally Fe-rich primitive subalkaline magmas.

As the next step, we have used compositional data on olivine phenocrysts to recognize whole-rock data that are most likely to represent "primary" ferropicrites, i.e., high-Fe-Mg melts instead of olivine cumulates (Table 5). Assuming a constant Fe^{2+}/Fe_{tot} of 0.9 and $K_D(Fe\text{-}Mg)^{ol\text{-}liq}$ of 0.35, the minimum Fo-content of olivine in equilibrium with ferropicritic liquids is Fo_{81}. Mineral chemical data on olivine in ferropicrites are rather scarce, however. The available data indicate that the depleted ferropicrites of Vestfjella (cf. section 7) and two of the Paraná-Etendeka samples (97SB63 and 97SB73) contain significant amounts of primitive olivine and can be considered as primary ferropicrites. In contrast, judging from the whole-rock and olivine compositions, the high MgO and FeO_{tot} contents of Paraná-Etendeka samples 96SB48, 97SB67, and 97SB68 with relatively Fe-rich olivine (Fo_{67} on average) may stem from olivine accumulation. A more specific olivine dataset for the ferropicrites from the Siberian Traps and Ahlmannryggen would be required to reliably evaluate their primary nature. In addition, accumulation of olivine in the ferropicrites of Madagascar, Greenland, and the enriched ferropicrites of Vestfjella cannot be assessed in this way due to the lack of published compositional data on olivine. The meimechites from Japan have high MgO (≥ 22 wt. %) and low Al_2O_3 and CaO (both ≤ 5 wt. %), and contain abundant pseudomorphed olivine phenocrysts (40–45 vol. %) indicative of cumulate rock (cf. Ichiyama et al., 2007), but the possible effect of olivine accumulation on FeO_{tot} contents cannot be reliably estimated without compositional data on olivine.

Table 5
Key characteristics of Phanerozoic rocks reported as ferropicrites

Location and samples	olivines *	LOI	Nb/Y	$(V/Lu)_N$	nature †
Vestfjella depleted type: AL/B14e-98, AL/B16-98, AL/WM1b-98	$Fo_{79–88\ (84)}$	1.1–3.8	0.4–0.5	1.9–2.2	primary
Paraná-Etendeka: 97SB63,97SB73	$Fo_{76–85\ (82)}$	0.9–1.6	0.9–1.1	1.2	primary
Paraná-Etendeka: 96SB48, 97SB67, 97SB68	$Fo_{64–81\ (67)}$	0.2–0.5	0.5–0.7	0.9–1.4	cumulate
Siberian Traps: SG-322301, SG-322332.7, 1F(18)	*$Fo_{72–81\ (78)}$*	7.4–8.1	0.4–1.0	1.1	cumulate?
Ahlmannryggen: Z1812.1, Z1813.1, Z1816.2	*$Fo_{70–86\ (?)}$*	1.7–2.6	0.2–0.3	0.8	uncertain
Vestfjella enriched type: AL/B20a-98, 14-KHG-90	-	4.4–5.5	0.7–0.8	1.3	uncertain
Madagascar: MAN90-45, MAN90-47	-	0–0.4	0.9–1.0	2.1–2.2	uncertain
East Greenland: MF91-57b, MF91-57c	-	3.5–3.6	-	1.4–1.7	uncertain, alkaline?
Japan: 040406-OG1, 040522-OG8, 040605-OG17, 040605-OG19	-	-	1.4–1.5	0.6–0.8	cumulate, alkaline?

Data sources for whole-rock geochemistry are given in section 10.1. LOI values are given in wt. %.
* Total range in group/formation/samples, calculated average in parentheses. Olivine data sources: Gibson et al., 2000 (supplementary data); Ryabov et al., 1977; Zolotukhin and Al'mukhamedov, 1991; Zolotukhin et al., 1991; Riley et al., 2005.
† Primary nature of the suite assessed (cf. section 10.1.; Fig. 10)

Several ferropicrites exhibit considerably high LOI values suggestive of strong alteration (Table 5). Secondary loss or gain of alkalis can have a pronounced effect on the normative compositions and complicates identification of subalkaline and alkaline rocks. Geochemical comparison suggests that ferropicrites can be distinguished from high-Fe-Mg nephelinites, basanites, meimechites and meimechite-related alkaline picrites with reasonable confidence using the Zr/Ti vs. Nb/Y classification diagram designed for altered and metamorphosed volcanic rocks (Fig. 10a). Ferropicrites typically exhibit low Nb/Y values (0.2–1.1) compared to alkaline high-Fe-

Mg rocks (1.2–4), whereas the meimechites of Japan show alkaline affinity based on high Nb/Y values (1.4–1.5) (Table 5; Fig. 10a). Furthermore, ferropicrites can be generally identified using a FeO_{tot}/CaO vs. SiO_2/Al_2O_3 diagram (Fig. 10b): Meimechites and related alkaline picrites exhibit notably high SiO_2/Al_2O_3 and highly variable FeO_{tot}/CaO and nephelinites and basanites define a relatively tight cluster at low SiO_2/Al_2O_3 and FeO_{tot}/CaO values. Ferropicrites, including the strongly altered samples from the Siberian Traps and Vestfjella, comprise a fairly well-defined group at intermediate SiO_2/Al_2O_3 and FeO_{tot}/CaO values. Two of the reported ferropicrite suites plot apart from the main group. The altered ferropicrites of Greenland plot within the field of nephelinites and basanites (Fig. 10b), but this affinity cannot be further evaluated using immobile trace elements due to lack of Nb data (Table 5). The strongly altered meimechitic samples of Japan define a distinct cluster at high SiO_2/Al_2O_3 and FeO_{tot}/CaO values.

In conclusion, although critical evaluation of the dataset of Phanerozoic ferropicrites is hampered by inadequate chemical data on olivine and uncertainties related to secondary alteration, we are able to identify likely examples of primary ferropicrites and cumulates, as well as several uncertain ferropicrite suites (Table 5). Three samples from Paraná-Etendeka are likely to represent olivine cumulates and the meimechites from Japan may represent cumulates or alkaline high-Fe-Mg melts; these rocks are discarded from our database and the subsequent discussion.

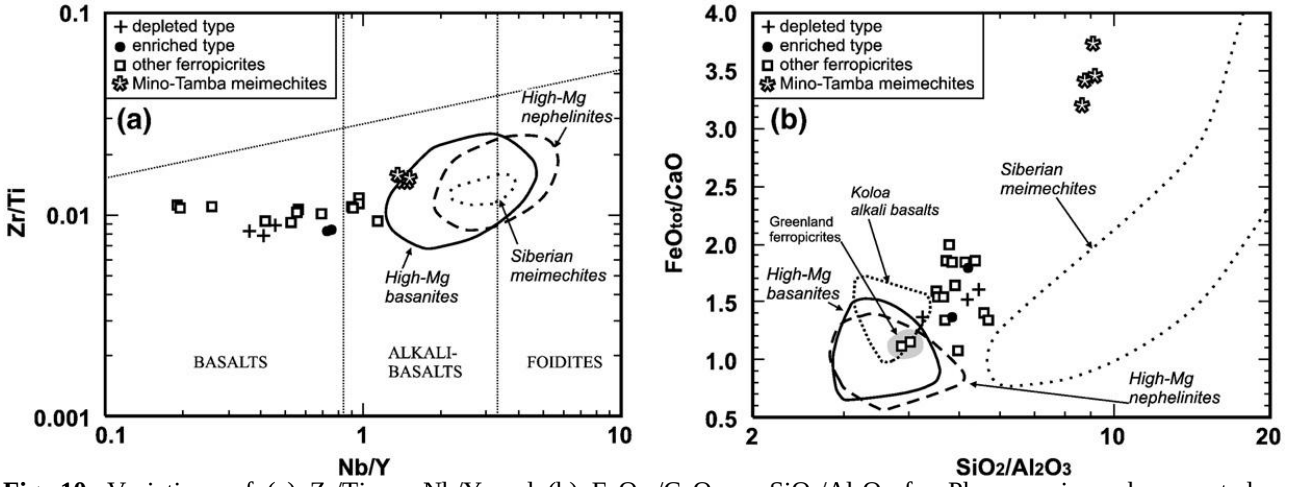

Fig. 10. Variations of (a) Zr/Ti vs. Nb/Y and (b) FeO_{tot}/CaO vs. SiO_2/Al_2O_3 for Phanerozoic rocks reported as ferropicrites. High-Mg nephelinites and basanites (MgO>10 wt.%; n>300; data compiled from GEOROC: http://georoc.mpch-mainz.gwdg.de/georoc/), Siberian meimechites and related alkaline picrites (n>50; Arndt et al., 1995; Fedorenko and Czamanske, 1997; Kogarko and Ryabchikov, 2000), and alkali basalts of the Koloa Volcanic Suite, Kauai, Hawaii (only in (b): n=20; Reiners and Nelson, 1998) are shown for comparison. Rock classification in (a) is after Pearce (1996).

10.2. Ferropicrite factors: evidence from global dataset

We have compared the REE and V geochemistry of ferropicrites and OIPs worldwide to evaluate the significance of high pressure and Fe-Ti gabbro component for generating ferropicrites (Fig. 9).

Ferropicrites show wide ranges and a broad positive correlation of $(La/Sm)_N$ and $(Sm/Yb)_N$ values (Fig. 9a). Compared to OIPs, most ferropicrites exhibit higher $(Sm/Yb)_N$ at given $(La/Sm)_N$. Furthermore, most ferropicrites have high primitive mantle-normalized $(V/Lu)_N$ values and mainly plot on the high $(V/Lu)_N$ side of the OIP field in Fig. 9b. Interpretation of incompatible element ratios of different magmatic suites is not straightforward due to possible effects of differentiation processes, and contamination in particular (Fig. 6). Although considerable lower crustal contamination has been associated with the Paraná-Etendeka suite (Gibson et al., 2000), most of the ferropicrites are considered to represent nearly uncontaminated magmas (Fram and Lesher, 1997;

Storey et al., 1997; Gibson et al., 2000; Riley et al., 2005; this study). Therefore, the prevalence of high $(Sm/Yb)_N$ in ferropicrites may well indicate generation of these magmas by relatively low-degree melting of garnet bearing sources at relatively high pressures. Importantly, anomalous high V contents are not likely to result from contamination and we regard high $(V/Lu)_N$ to indicate presence of an Fe-Ti gabbro component in many ferropicrites.

Two ferropicrite suites show geochemical signatures that are indistinguishable from those of OIP and have compositional features that do not readily fit into our model. One of the Siberian Traps ferropicrites has relatively high $(V/Lu)_N$ value indicative of Fe-Ti gabbro-bearing sources (V data for the other two Siberian Traps ferropicrites are not available), but it plots in the OIP field with respect to $(La/Sm)_N$ and $(Sm/Yb)_N$ (Fig. 9a). On the other hand, the Ahlmannryggen ferropicrites have low, OIP-like $(V/Lu)_N$ combined with low $(La/Sm)_N$ at given $(Sm/Yb)_N$. We do not interpret these anomalous features further, but they may well record different melting conditions and/or REE characteristics of their mantle sources. It should also be remembered that the primary nature of these unusual ferropicrites has not been confirmed (cf. Table 5).

Based on the global ferropicrite dataset, and variations in $(La/Sm)_N$, $(Sm/Yb)_N$, and $(V/Lu)_N$ in particular, we propose that the principal difference between OIPs and ferropicrites is that the latter included an exceptionally Fe-rich eclogite source component and were derived as low-degree melts at relatively high pressures. These ferropicrite factors are generally, but not necessarily, coupled due to the compositional dependence of solidus temperatures. It is possible that some ferropicrites simply represent incipient melts of common pyroxenite sources. However, the characteristic positive V anomalies of many ferropicrites (Fig. 9) indicate recycled Fe-Ti gabbro to be a significant source component, although in some cases other Fe-enriched components of recycled oceanic crust, such as ferrobasalts (e.g. Byerly et al., 1976), could have been involved (cf. Ichiyama et al., 2006). Fe-Ti gabbros represent a common, albeit volumetrically minor component of the oceanic crust (e.g., Niu et al., 2002; Thy, 2003). Ferrobasalts occur abundantly only in fast-spreading oceanic ridges (e.g., Thy 1985) and, therefore, are expected to be less frequently incorporated into upwelling mantle.

11. Ferropicrites and mantle plumes

The generation of ferropicrites has been commonly, but not unanimously (Hanski, 1992), linked to mantle plumes (e.g., Gibson et al., 2000; Gibson 2002; Riley et al., 2005; Ichiyama et al., 2006). We have estimated the mantle source temperatures of ferropicrites using olivine and whole-rock data on the depleted ferropicrites of Vestfjella. The simplified composition-independent model of Putirka (2005) indicates olivine-liquid equilibration temperatures of 1510–1580 ºC for ferropicrites (Fig. 11). This temperature range is marginally lower than that of common Hawaiian picrites (1570–1620 ºC; Fig. 11), but it exceeds that of MOR basalts (< 1470 ºC; Putirka, 2005), and supports derivation of ferropicrites from anomalous hot mantle material that may correspond to thermally driven mantle plumes. We emphasize that the purpose of Fig. 11 is not to provide exact mantle potential temperatures for ferropicrite sources, but to compare ferropicrites with common plume-derived melts. A more elaborate modeling of mantle potential temperatures, with additional factors taking into account the effects of, e.g., H_2O contents and decompression, would be expected to yield even higher temperatures for ferropicrites and OIPs (e.g., T_p Hawaii ~1690 °C) relative to MORBs (T_p ~1450–1480 °C; cf. Putirka, 2005).

The presence of ferropicrites close to the base of CFB successions has been linked to generation and preservation of unusually Fe-rich melts in mantle plume starting-heads due to relatively low solidus temperatures of ferropicrite sources and less effective overprinting of ferropicritic melts by peridotite melting compared to hotter interiors of plume heads and plume tails (Gibson, 2002). Based on the ferropicrite factors presented above, we consider that, theoretically, generation and preservation of ferropicritic melts could be also expected to relate to regions of

limited melting in the peripheral parts of plume tails. Accordingly, ferropicrites might be able to intrude the crust and erupt under favorable conditions at different stages of hotspot evolution. In the light of current evidence, it is possible that at least some of the Karoo-related ferropicrites were not emplaced during the initial stage of magmatism: (1) The Karoo-related ferropicrites are found only as dikes crosscutting CFB lavas and gabbros (Vestfjella) or Precambrian basement (Ahlmannryggen; Riley et al., 2005). (2) Unambiguous age data for Karoo-related ferropicrites are currently not available (Zhang et al., 2003b; Riley et al., 2005). (3) Paleomagnetic data show that the enriched ferropicrite dikes of Vestfjella exhibit a reversed magnetic polarity (sample A18/Ba60 in Peters, 1989), whereas the main part of the Karoo CFBs, including the wall-rock low-Ti lavas in Vestfjella, show normal polarity (Hargraves et al., 1997; Peters, 1989). Nevertheless, all of the currently known Phanerozoic ferropicrite suites (Table 5) can be associated with magmatism related to plume heads and ferropicrites related to plume tails have not been positively identified.

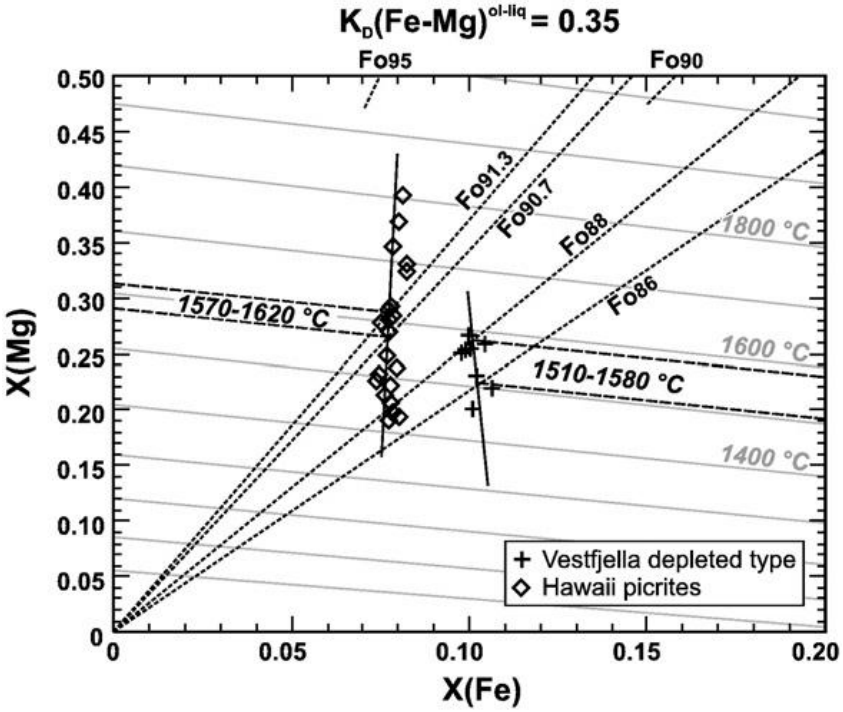

Fig. 11. Olivine-liquid thermometer model for the Vestfjella ferropicrites (depleted type dikes 4 and 5) and Hawaiian picrites (Norman and Garcia, 1999). X(Mg) and X(Fe) are cation fractions of Mg and Fe^{2+} assuming Fe^{2+}/Fe_{tot}=0.9. Isotherms have been calculated using the composition-independent equations of Putirka (2005). Stippled lines indicate olivine compositions and dashed isotherms show temperature ranges defined by the intersections of observed olivine phenocrysts compositions (Green et al., 2001; this study) and olivine-controlled liquid lines estimated based on whole-rock data. Compositional factors (alkalis, H_2O), heat of fusion, and decompression along mantle adiabat are not incorporated into the model (cf. Putirka, 2005).

Whether or not ferropicrites exist on oceanic islands is of key importance to understanding of ferropicritic magmatism. According to Tuff et al. (2005), oceanic ferropicrites have not been found because (1) the small-volume Fe-rich melts get diluted in the areas of thin lithosphere by voluminous melts from "common" OIP sources, or (2) the early evolutionary stages of plumes are simply not represented in the OIP record. Volcanic rocks on oceanic islands are characterized by significant geochemical heterogeneity which is especially strong among the pre-shield and post-shield stage lavas that represent less-voluminous low-degree melts derived from the peripheral parts of plume tails (e.g., Reiners and Nelson, 1998). Such volcanic suites also include high-Fe-Mg rocks that show geochemical affinities to ferropicrites, but typically have relatively lower SiO_2 and higher Al_2O_3 values (cf. Fig. 10b). These particular dissimilarities are compatible with lower degree of melting at shallower depths, respectively, and do not necessarily require different mantle sources.

We suggest that, similar to ferropicrites, some of the oceanic plume-derived high-Fe-Mg rocks could have been generated from Fe-Ti gabbro -bearing mantle sources. For example, Reiners and Nelson (1998) have reported post-shield high-Mg alkali basalts with unusually high FeO_{tot} (up to 15 wt. %) from Hawaii (The Koloa Volcanic Suite, Kauai). These rocks are similar to ferropicrites in having relatively high SiO_2 (~44 wt. %), low $Na_2O + K_2O$ (≤ 3 wt. %), and high $(La/Sm)_N$ (1.8–2.6), $(Sm/Yb)_N$ (3.5–6.3), and $(V/Lu)_N$ (1.0–1.6), and in containing primitive olivines (Fo_{85-88}) typical of primary magmas. Their substantially high LOI values (3.5–9.4 wt. %) indicate strong alteration, but, because of inadequate geochemical data, Nb/Y values cannot be utilized to further assess their alkalinity. In Fig. 10b, they partially overlap the fields of ferropicrites and nephelinites/basanites. Based on the ferropicritic characteristics of the Koloa rocks, high FeO_{tot} and $(V/Lu)_N$ in particular, they may represent melting of Fe-Ti gabbro-bearing sources in plume tails and are well worthy of a closer look in search of oceanic correlatives of ferropicrites.

12. Ferropicrites and Karoo magmatism

The presence of ferropicrites as dikes at Vestfjella and Ahlmannryggen (Harris et al., 1991; Riley et al., 2005) raises questions regarding the timing, duration, and significance of ferropicritic magmatism in the Karoo LIP. Given that the age relationship between the ferropicrites of Vestfjella and Ahlmannryggen have not been reliably established and that the distinctive geochemical signatures of these suites indicate different mantle sources and melting conditions for them (Figs. 6, 9 and 12), it is possible that ferropicrite magmas were generated at different stages of Karoo magmatism. Evidence of early stage ferropicrite magmatism is lacking in the lava stratigraphy (e.g. Erlank, 1984; Harris et al., 1990; Sweeney et al., 1994; Marsh et al., 1997; Luttinen & Furnes, 2000; Jourdan et al., 2007a), but this could result from the tendency of high-density picrite magmas to accumulate in the lower crust or from unrepresentative sampling of the voluminous but patchy volcanic record. In addition, strong lithospheric contamination hampers the recognition of possible ferropicritic parental melts for the Karoo magma types, although the relatively low FeO_{tot} contents of the Karoo magmas do not favor this possibility. One exception is the so-called high-Fe basalt suite in the upper part of the Lebombo lava succession (Sweeney et al., 1994). They have geochemical similarities with the enriched ferropicrites of Vestfjella (Figs. 5 and 12) and could represent differentiates of ferropicritic parental magmas. Judging from their higher La/Nb and lower initial ε_{Nd} values compared to the enriched ferropicrites (Figs. 5 and 12), however, the high-Fe basalts include a lithospheric component that renders reliable geochemical correlation ambiguous.

In summary, correlatives or magmatic differentiates of the Vestfjella ferropicrites have not been positively identified in the Karoo LIP. Based on the available data, ferropicritic magmas may have been generated from distinctive mantle sources, possibly during several stages of Karoo magmatism, but reliable geochronological data are required to establish the intrusive ages of the ferropicrites. Although ferropicrites may not represent a volumetrically significant magma type, the OIP-like geochemical traits (Figs. 4 and 5) and the high temperatures of the ferropicritic primary melts (Fig. 11) support a plume source for the Karoo LIP (cf. Riley et al., 2005), and contribute to the debate on the nature of hotspots and the existence of mantle plumes and their significance as sources of LIP magmatism (e.g. Foulger et al., 2005).

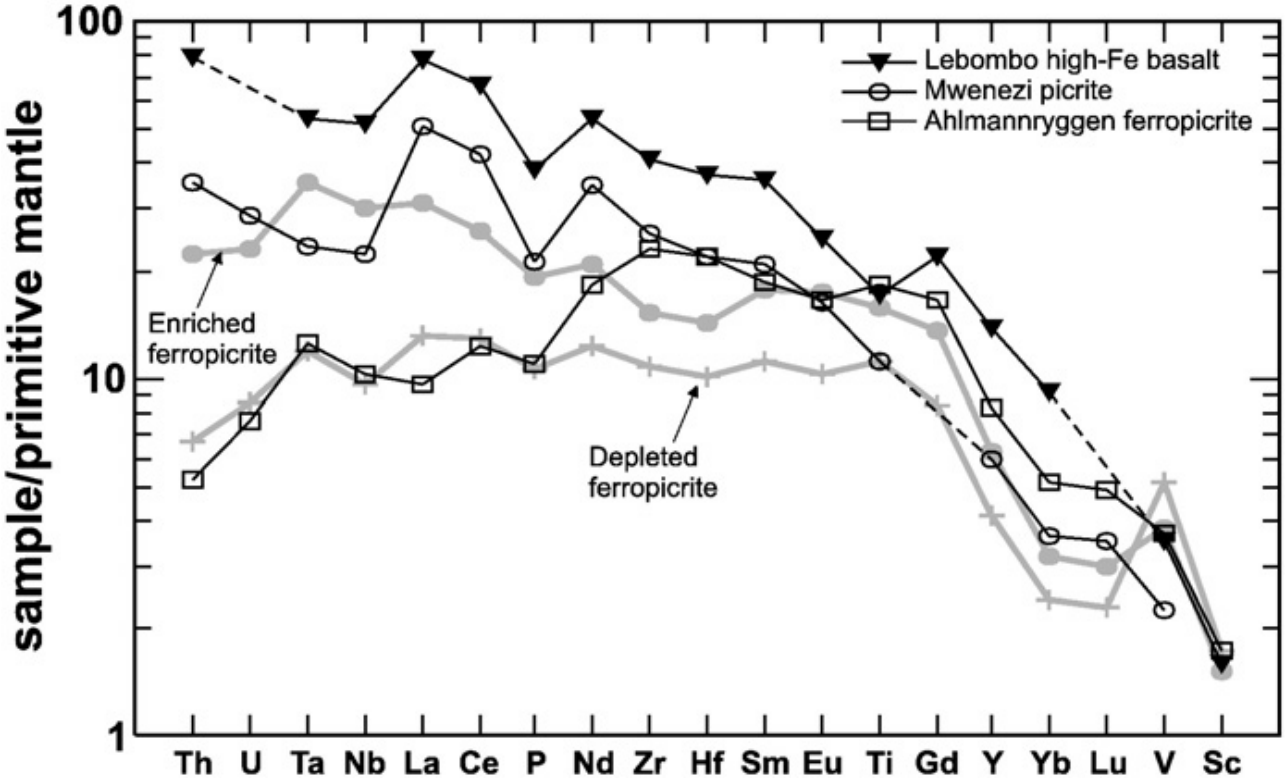

Fig. 12. Primitive mantle-normalized incompatible element patterns for depleted (sample AL/WM1b-98) and enriched (sample AL/B20a-98) ferropicrites of Vestfjella, high-Fe lava from central Lebombo (RSC-038; Sweeney et al.,1994), Mwenezi picrite (N-117; Ellam and Cox, 1989), and ferropicrite from Ahlmannryggen (Z1812-1;Riley et al.,2005). Normalizing values as in Fig. 4.

13. Conclusions

Our results on the ferropicritic (FeO_{tot} > 13 wt. %, MgO 12–18 wt. %) dikes and their differentiates (basaltic and meimechitic dikes) in Vestfjella, western DML, Antarctica, and analysis of a global ferropicrite dataset, lead to the following conclusions:

1. Geochemically, the Vestfjella ferropicrites have broad affinities to oceanic island basalts and picrites and can be divided into two distinct types: (a) Depleted ferropicrites less enriched in incompatible elements and with relatively low $(La/Sm)_N$ and $(Sm/Yb)_N$, high $(V/Lu)_N$, ε_{Sr} from -18 to -19, and ε_{Nd} from +7 to +8. (b) Enriched ferropicrites more enriched in most incompatible elements and with higher $(La/Sm)_N$ and $(Sm/Yb)_N$, but lower $(V/Lu)_N$ values, ε_{Sr} from 0 to +1, and ε_{Nd} from +3 to +4.

2. Combined olivine, whole-rock, and isotopic data show that at least the depleted ferropicrites represent Fe-rich, near-primary subalkaline to mildly alkaline melt compositions. The immobile incompatible element ratios of the dikes have not been significantly affected by subsolidus alteration, fractional crystallization, or contamination, and they can be used for characterization of the primary melts and the mantle sources of ferropicrites.

3. The major element data of the Vestfjella ferropicrites are compatible with garnet-bearing pyroxenitic mantle sources recently suggested for other ferropicrites and OIB. The geochemical signature of the depleted ferropicrites, specifically the strong enrichment of V, is remarkably similar to that of oceanic Fe-Ti gabbros and indicates such a component in the pyroxenite source. Geochemical modeling supports this interpretation and indicates a similar source component in most ferropicrites. The enriched ferropicrites presumably record an Fe-

rich source component, e.g., ferrobasalt, but their high Fe contents could also reflect relatively low-degree melting at higher pressure, as indicated by the high $(La/Sm)_N$ and $(Sm/Yb)_N$ ratios.

4. The Vestfjella ferropicrites lack geochemical correlatives in the Karoo province; specifically, their geochemical signatures are distinct from those of the recently reported Ahlmannryggen ferropicrites. Markedly high mantle potential temperatures, derived from olivine-melt equilibria for the depleted ferropicrites, support involvement of plume sources during Karoo magmatism.

5. Petrogenetic research on ferropicrites requires a coherent classification scheme and critical evaluation of possible effects of olivine accumulation and alteration. The shortcomings of the currently available data, most notably the lack of compositional data on olivine phenocrysts, undermine reliable identification of samples representing ferropicrite melts.

Acknowledgements
We thank Tapani Rämö for his comments on an earlier draft of this manuscript and Hannu Huhma from the Geological Survey of Finland for invaluable help with the isotope analyses. Editorial feedback by Andrew Kerr and the constructive reviews by Sally Gibson and Teal Riley facilitated substantial improvement of the paper. We thank the FINNARP crew for invaluable field assistance and Henrik Grind and Mika Räisänen for providing dike samples and field data. Diane Johnson, Rick Conrey, and Charles Knaack from the GeoAnalytical Laboratory, Washington State University, performed the XRF and ICP-MS analyses, Stephen Reed, University of Cambridge, ran the olivine analyses, and Helena Korkka and Quality Thin Sections prepared the thin sections. Our research has been funded by the Academy of Finland (Grant no. 210640 for JSH and 111930 for AVL).

References

Arndt, N., Lehnert, K., Vasil'ev, Y., 1995. Meimechites: highly magnesian lithosphere-contaminated alkaline magmas from deep subcontinental mantle. Lithos 34 (1-3), 41-59.

Arndt, N.T., Todt, W., Chauvel, C., Tapfer, M., Weber, K., 1991. U-Pb zircon age and Nd isotopic composition of granitoids, charnockites and supracrustal rocks from Heimefrontfjella, Antarctica. Geologische Rundschau 80, 759-777.

Barton, J.M.Jr., Klemd, R., Allsopp, H.L., Auret, S.H., Copperthwaite, Y.E., 1987. The geology and geochronology of the Annandagstoppane granite, Western Dronning Maud Land, Antarctica. Contributions to Mineralogy and Petrology 97 (4), 488-496.

Becker, H., Jochum, K.P., Carlson, R.W., 2000. Trace element fractionation during dehydration of eclogites from high-pressure terranes and the implications for element fluxes in subduction zones. Chemical Geology 163 (1-4), 65-99.

Bohrson, W.A., Spera, F.J., 2001. Energy-constrained open-system magmatic processes; II, Application of energy-constrained assimilation-fractional crystallization (EC-AFC) model to magmatic systems. Journal of Petrology 42 (5), 1019-1041.

Boudreau, A.E., 1999. PELE; a version of the MELTS software program for the PC platform. Computers and Geosciences 25 (2), 201-203.

Byerly, G.R., Melson, W.G., Vogt, P.R., 1976. Rhyodacites, andesites, ferro-basalts and ocean tholeiites from the Galapagos spreading center. Earth and Planetary Science Letters 30 (2), 215-221.

Coogan, L.A., MacLeod, C.J., Dick, H.J.B., Edwards, S.J., Kvassnes, A., Natland, J.H., Robinson, P.T., Thompson, G., O'Hara, M.J., 2001. Whole-rock geochemistry of gabbros from the Southwest Indian Ridge: constraints on geochemical fractionations between the upper and lower oceanic crust and magma chamber processes at (very) slow-spreading ridges. Chemical Geology 178 (1-4), 1-22.

Corner, B., 1994. Geological evolution of western Dronning Maud Land within a Gondwana framework: Geophysics subprogramme. Final project report to SACAR. Department of Geophysics, Whitwaterstrand University, South Africa. 21 pages.

Cox, K.G., Bristow, J.W., 1984. The Sabie River Basalt Formation of the Lebombo Monocline and South-east Zimbabwe. In: Erlank, A.J. (Ed.), Petrogenesis of the volcanic rocks of the Karoo Province. Geological Society of South Africa, Special Publication 13, pp. 125-147.

DePaolo, D.J., 1981. Trace element and isotopic effects of combined wallrock assimilation and fractional crystallization. Earth and Planetary Science Letters 53 (2), 189-202.

Duncan, A.R., Hooper, P.R., Rehacek, J., Marsh, J.S., Duncan, A.R., 1997. The timing and duration of the Karoo igneous event, southern Gondwana. Journal of Geophysical Research 102 (B8), 18127-18138.

Ellam, R.M., Cox, K.G., 1989. A Proterozoic lithospheric source for Karoo magmatism; evidence from the Nuanetsi picrites. Earth and Planetary Science Letters 92 (2), 207-218.

Ellam, R.M., Cox, K.G., 1991. An interpretation of Karoo picrite basalts in terms of interaction between asthenospheric magmas and the mantle lithosphere. Earth and Planetary Science Letters 105 (1-3), 330-342.

Erlank, A.J. (Ed.), 1984. Petrogenesis of the volcanic rocks of the Karoo Province. Geological Society of South Africa, Special Publication 13. 395 pages.

Fedorenko, V., Czamanske, G.K., 1997. Results of new field and geochemical studies of the volcanic and intrusive rocks of the Maymecha-Kotuy area, Siberian flood-basalt province, Russia. International Geology Review 39 (6), 479-531.

Foley, S., 1992. Vein-plus-wall-rock melting mechanisms in the lithosphere and the origin of potassic alkaline magmas. Lithos 28 (3-6), 435-453.

Foulger, G.R., Natland, J.H., Presnall, D.C., Anderson, D.L. (Eds.), 2005. Plates, plumes, and paradigms. Geological Society of America, Special Publication 388, Boulder, CO, United States. 881 pages.

Fram, M.S., Lesher, C.E., 1997. Generation and polybaric differentiation of east Greenland early tertiary flood basalts. Journal of Petrology 38 (2), 231-275.

Francis, D., Ludden, J., Johnstone, R., Davis, W., 1999. Picrite evidence for more Fe in Archean mantle reservoirs. Earth and Planetary Science Letters 167 (3-4), 197-213.

Gaffney, A.M., 2002. Environments of crystallization and compositional diversity of Mauna Loa xenoliths. Journal of Petrology 43 (6), 963-980.

Gibson, S.A., 2002. Major element heterogeneity in Archean to Recent mantle plume starting-heads. Earth and Planetary Science Letters 195 (1-2), 59-74.

Gibson, S.A., Thompson, R.N., Dickin, A.P., 2000. Ferropicrites; geochemical evidence for Fe-rich streaks in upwelling mantle plumes. Earth and Planetary Science Letters 174 (3-4), 355-374.

Govindaraju, K., 1994. 1994 Compilation of Working Values and Sample Description for 383 Geostandards. Geostandards Newsletter 18, 15-53.

Green, D.H., Falloon, T., Eggins, S.M., Yaxley, G.M., 2001. Primary magmas and mantle temperatures. European Journal of Mineralogy 13 (3), 437-451.

Halliday, A.N., Lee, D., Tommasini, S., Davies, G.R., Paslick, C.R., Fitton, J.G., James, D.E., 1995. Incompatible trace elements in OIB and MORB and source enrichment in the sub-oceanic mantle. Earth and Planetary Science Letters 133 (3-4), 379-395.

Hanski, E.J., 1992. Petrology of the Pechenga ferropicrites and cogenetic Ni-bearing gabbro-wehrlite intrusions, Kola Peninsula, Russia. Geological Survey of Finland, Bulletin 367, 192 pages.

Hanski, E.J., Smolkin, V.F., 1989. Pechenga ferropicrites and other early Proterozoic picrites in the eastern part of the Baltic Shield. Precambrian Research 45 (1-3), 63-82.

Hanski, E.J., Smolkin, V.F., 1995. Iron- and LREE-enriched mantle source for early Proterozoic intraplate magmatism as exemplified by the Pechenga ferropicrites, Kola Peninsula, Russia. Lithos 34 (1-3), 107-125.

Hargraves, R.B., Rehacek, J., Hooper, P.R., 1997. Palaeomagnetism of the Karoo igneous rocks in Southern Africa. South African Journal of Geology 100 (3), 195-212.

Harris, C., Marsh, J.S., Duncan, A.R., Erlank, A.J., 1990. The petrogenesis of the Kirwan Basalts of Dronning Maud Land, Antarctica. Journal of Petrology 31 (2), 341-369.

Harris, C., Watters, B.R., Groenewald, P.B., 1991. Geochemistry of the Mesozoic regional basic dykes of western Dronning Maud Land, Antarctica. Contributions to Mineralogy and Petrology 107 (1), 100-111.

Hauri, E.H., Wagner, T.P., Grove, T.L., 1994. Experimental and natural partitioning of Th, U, Pb and other trace elements between garnet, clinopyroxene and basaltic melts. Chemical Geology 117 (1-4), 149-166.

Hawkesworth, C.J., Marsh, J.S., Duncan, A.R., Erlank, A.J., Norry, M.J., 1984. The role of continental lithosphere in the generation of the Karoo volcanic rocks: evidence from combined Nd- and Sr-isotope studies. In: Erlank, A.J. (Ed.), Petrogenesis of the volcanic rocks of the Karoo Province. Geological Society of South Africa, Special Publication 13, pp. 341-354.

Herzberg, C., 2006. Petrology and thermal structure of the Hawaiian plume from Mauna Kea volcano. Nature 444, 605-609.

Hirose, K., Kawamoto, T., 1995. Hydrous partial melting of lherzolite at 1 GPa; the effect of H_2O on the genesis of basaltic magmas. Earth and Planetary Science Letters 133 (3-4), 463-473.

Hirschmann, M.M., Kogiso, T., Baker, M.B., Stolper, E.M., 2003. Alkalic magmas generated by partial melting of garnet pyroxenite. Geology (Boulder) 31 (6), 481-484.

Hofmann, A.W., White, W.M., 1982. Mantle plumes from ancient oceanic crust. Earth and Planetary Science Letters 57 (2), 421-436.

Hunter, D.R., Smith, R.G., Sleigh, D.W.W., 1992. Geochemical studies of Archaean granitoid rocks in the Southeastern Kaapvaal Province: implications for crustal development. Journal of South African Earth Sciences 15, 127-151.

Ichiyama, Y., Ishiwatari, A., Hirahara, Y., Shuto, K., 2006. Geochemical and isotopic constraints on the genesis of the Permian ferropicritic rocks from the Mino-Tamba belt, SW Japan. Lithos 89 (1-2), 47-65.

Ichiyama, Y., Ishiwatari, A., Koizumi, K., Ishida, Y., Machi, S., 2007. Olivine-spinifex basalt from the Tamba Belt, Southwest Japan; evidence for Fe- and high field strength element-rich ultramafic volcanism in Permian Ocean. Island Arc 16 (3), 493-503.

Jacobs, J., Bauer, W., Fanning, C.M., 2003. New age constraints for Grenville-age metamorphism in western central Dronning Maud Land (East Antarctica), and implications for the palaeogeography of Kalahari in Rodinia. International Journal of Earth Sciences 92 (3), 301-315.

Jacobs, J., Fanning, C.M., Henjes-Kunst, F., Olesch, M., Paech, H., 1998. Continuation of the Mozambique Belt into East Antarctica; Grenville-age metamorphism and polyphase Pan-African high-grade events in central Dronning Maud Land. Journal of Geology 106 (4), 385-406.

Johnson, D.M., Hooper, P.R., Conrey, R.M., 1999. XRF Analysis of Rocks and Minerals for Major and Trace Elements on a Single Low Dilution Li-tetraborate Fused Bead. Advances in X-ray Analysis 41, 843-867.

Johnson, K.T.M., 1994. Experimental cpx/ and garnet/melt partitioning of REE and other trace elements at high pressures; petrogenetic implications. V. M. Goldschmidt Conference; extended abstracts. Mineralogical Magazine 58A (A-K), 454-455.

Jourdan, F., Bertrand, H., Schärer, U., Blichert-Toft, J., Feraud, G., Kampunzu, A.B., 2007a. Major and trace element and Sr, Nd, Hf, and Pb isotope compositions of the Karoo large igneous province, Botswana–Zimbabwe: lithosphere vs mantle plume contribution. Journal of Petrology 48 (6), 1043-1077.

Jourdan, F., Feraud, G., Bertrand, H., Watkeys, M.K., 2007b. From flood basalts to the inception of oceanization: Example from the $^{40}Ar/^{39}Ar$ high-resolution picture of the Karoo large igneous province. Geochemistry, Geophysics, Geosystems 8, doi:10.1029/2006GC001392

Kawamoto, T., Holloway, J.R., 1997. Melting temperature and partial melt chemistry of H_2O-saturated mantle peridotite to 11 gigapascals. Science 276, 240-243.

Klemme, S., Prowatke, S., Hametner, K., Guenther, D., 2005. Partitioning of trace elements between rutile and silicate melts; implications for subduction zones. Geochimica et Cosmochimica Acta 69 (9), 2361-2371.

Knaack, C., Cornelius, S.B., Hooper, P.R., 1994. Trace Element Analyses of Rocks and Minerals by ICP-MS. GeoAnalytical Lab. (http://www.wsu.edu/~geolab/note/icpms.html), Washington State University.

Kogarko, L.N., Ryabchikov, I.D., 2000. Geochemical evidence for meimechite magma generation in the subcontinental lithosphere of polar Siberia. Journal of Asian Earth Sciences 18 (2), 195-203.

Kogiso, T., Hirschmann, M.M., Frost, D.J., 2003. High-pressure partial melting of garnet pyroxenite; possible mafic lithologies in the source of ocean island basalts. Earth and Planetary Science Letters 216 (4), 603-617.

Lawver, L.A., Gahagan, L.M., Coffin, M.F., 1992. Development of paleoseaways around Antarctica. In: Kennett, J. P., Warnke, D. A. (Eds.), The Antarctic paleoenvironment: a perspective on global change. Antarctic Research Series 56, pp. 7-30.

Le Bas, M.J., 2000. IUGS reclassification of the high-Mg and picritic volcanic rocks. Journal of Petrology 41 (10), 1467-1470.

Lightfoot, P.C., Hawkesworth, C.J., Hergt, J., Naldrett, A.J., Gorbachev, N.S., Fedorenko, V.A., Doherty, W., 1993. Remobilisation of the continental lithosphere by a mantle plume; major-, trace-element, and Sr-, Nd-, and Pb-isotope evidence from picritic and tholeiitic lavas of the Noril'sk District, Siberian Trap, Russia. Contributions to Mineralogy and Petrology 114 (2), 171-188.

Luttinen, A.V., Furnes, H., 2000. Flood basalts of Vestfjella; Jurassic magmatism across an Archaean-Proterozoic lithospheric boundary in Dronning Maud Land, Antarctica. Journal of Petrology 41 (8), 1271-1305.

Luttinen, A.V., Zhang, X., Foland, K.A., 2002. 159 Ma Kjakebeinet lamproites (Dronning Maud Land, Antarctica) and their implications for Gondwana breakup processes. Geological Magazine 139 (5), 525-539.

Luttinen, A.V., Ramo, O.T., Huhma, H., 1998. Neodymium and strontium isotopic and trace element composition of a Mesozoic CFB suite from Dronning Maud Land, Antarctica; implications for lithosphere and asthenosphere contributions to Karoo magmatism. Geochimica et Cosmochimica Acta 62 (15), 2701-2714.

Marsh, J.S., Hooper, P.R., Rehacek, J., Duncan, R.A., Duncan, A.R., 1997. Stratigraphy and age of Karoo basalts of Lesotho and implications for correlations within the Karoo igneous province. In: Mahoney, J.J., Coffin, M.F. (Eds.), Large igneous provinces; continental, oceanic, and planetary flood volcanism. Geophysical Monograph vol. 100, American Geophysical Union, United States, pp. 247-272.

McDonough, W.F., Frey, F.A., 1989. Rare earth elements in upper mantle rocks. In: Lipin, B.R., McKay, G.A. (Eds.), Geochemistry and mineralogy of rare earth elements, Reviews in Mineralogy 21, Mineralogical Society of America, pp. 100-145.

McDonough, W.F., Sun, S.S., 1995. The composition of the Earth. Chemical Geology 120 (3-4), 223-253.

Menzies, M.A., Murthy, V.M., 1980. Enriched mantle: Nd and Sr isotopes in diopsides from kimberlite nodules. Nature 283, 634-636.

Moyes, A.B., Krynauw, J.R., Barton, J.M.,Jr, 1995. The age of the Ritscherflya Supergroup and Borgmassivet Intrusions, Dronning Maud Land, Antarctica. Antarctic Science 7 (1), 87-97.

Niu, Y., Gilmore, T., Mackie, S., Greig, A., Bach, W., 2002. Mineral chemistry, whole-rock compositions, and petrogenesis of Leg 176 gabbros: data and discussion. In: Natland, J.H., Dick, H.J.B., Miller, D.J., Von Herzen, R.P. (Eds.), Proceedings, Ocean Drilling Program Scientific Results, vol. 176. Ocean Drilling Program, College Station, TX, pp. 1-60 [Online].

Norman, M.D., Garcia, M.O., 1999. Primitive magmas and source characteristics of the Hawaiian Plume; petrology and geochemistry of shield picrites. Earth and Planetary Science Letters 168 (1-2), 27-44.

O'Hara, M.J., 1968. The bearing of phase equilibria studies in synthetic and natural systems on the origin and evolution of basic and ultrabasic rocks. Earth Science Reviews 4 (2), 69-133.

Pearce, J.A., 1996. A user's guide to basalt discrimination diagrams. In: Wyman, D.A. (Ed.), Trace element geochemistry of volcanic rocks: applications for massive sulphide exploration. Geological Association of Canada, Short Course Notes, vol. 12, 79-113.

Peters, M., 1989. Die Vulkanite im westlichen und mittleren Neuschwabenland, Vestfjella und Ahlmannryggen, Antarktika; Petrographie, Geochemie, Geochronologie, Palaeomagnetismus, geotektonische Implikationen. Berichte zur Polarforschung 61, Alfred Wegener-Institut für Polar- und Maareforschung, Bremerhaven, 186 pages. (In German)

Putirka, K., 1999. Melting depths and mantle heterogeneity beneath Hawaii and the East Pacific Rise; constraints from Na/Ti and rare earth element ratios. Journal of Geophysical Research 104 (B2), 2817-2829.

Putirka, K.D., 2005. Mantle potential temperatures at Hawaii, Iceland, and the mid-ocean ridge system, as inferred from olivine phenocrysts; evidence for thermally driven mantle plumes. Geochemistry, Geophysics, Geosystems 6, doi:10.1029/2005GC000915

Reiners, P.W., Nelson, B.K., 1998. Temporal-compositional-isotopic trends in rejuvenated-stage magmas of Kauai, Hawaii, and implications for mantle melting processes. Geochimica et Cosmochimica Acta 62 (13), 2347-2368.

Rhodes, J.M., Vollinger, M.J., 2004. Composition of basaltic lavas sampled by phase-2 of the Hawaii Scientific Drilling Project; geochemical stratigraphy and magma types. Geochemistry, Geophysics, Geosystems 5, doi:10.1029/2002GC000434

Riley, T.R., Leat, P.T., Curtis, M.L., Millar, I.L., Duncan, R.A., Fazel, A., 2005. Early-Middle Jurassic Dolerite Dykes from Western Dronning Maud Land (Antarctica): Identifying Mantle Sources in the Karoo Large Igneous Province. Journal of Petrology 46 (7), 1489-1524.

Rudnick, R.L., Fountain, D.M., 1995. Nature and composition of the continental crust: a lower crustal perspective. Reviews of Geophysics 33 (3), 267-309.

Rudnick, R.L., Gao, S., 2003. The Composition of the Continental Crust. In: Rudnick, R.L. (Ed.), The Crust, Treatise on Geochemistry vol. 3, Elsevier-Pergamon, Oxford, pp. 1-64.

Ryabov, V.V., Bakumenko, I.T., Fominykh, I.M., 1977. Dendritic megacrystals of clinopyroxene in trap rocks of the Norilsk region and some questions concerning their formation. In: Sobolev, V.S. (Ed.), Data on genetic mineralogy and petrology. Nauka, Novosibirsk, pp. 47-74. (in Russian)

Salters, V.J.M., Stracke, A., 2004. Composition of the depleted mantle. Geochemistry, Geophysics, Geosystems 5, doi:10.1029/2003GC000597

Sinton, J.M., Detrick, R.S., 1992. Mid-ocean ridge magma chambers. Journal of Geophysical Research 97 (B1), 197-216.

Sobolev, A.V., Hofmann, A.W., Kuzmin, D.V., Yaxley, G.M., Arndt, N.T., Chung, S., Danyushevsky, L.V., Elliott, T., Frey, F.A., Garcia, M.O., Gurenko, A.A., Kamenetsky, V.S., Kerr, A.C., Krivolutskaya, N.A., Matvienkov, V.V., Nikogosian, I.K., Rocholl, A., Sigurdsson, I.A., Sushchevskaya, N.M., Teklay, M., 2007. The amount of recycled crust in sources of mantle-derived melts. Science 316, 412-417.

Sobolev, A.V., Hofmann, A.W., Nikogosian, I.K., 2000. Recycled oceanic crust observed in "ghost plagioclase" within the source of Mauna Loa lavas. Nature 404, 986-990.

Sobolev, A.V., Hofmann, A.W., Sobolev, S.V., Nikogosian, I.K., 2005. An olivine-free mantle source of Hawaiian shield basalts. Nature 434, 590-597.

Spandler, C., Hermann, J., Arculus, R., Mavrogenes, J., 2004. Geochemical heterogeneity and element mobility in deeply subducted oceanic crust; insights from high-pressure mafic rocks from New Caledonia. Chemical Geology 206 (1-2), 21-42.

Stone, W.E., Crocket, J.H., Dickin, A.P., Fleet, M.E., 1995. Origin of Archean ferropicrites: geochemical constraints from the Boston Creek Flow, Abitibi greenstone belt, Ontario, Canada. Chemical Geology 121 (1-4), 51-71.

Stone, W.E., Deloule, E., Larson, M.S., Lesher, C.M., 1997. Evidence for hydrous high-MgO melts in the Precmabrian. Geology (Boulder) 25 (2), 143-146.

Storey, M., Mahoney, J.J., Saunders, A.D., 1997. Cretaceous basalts in Madagascar and the transition between plume and continental lithosphere mantle sources. In: Mahoney, J.J., Coffin, M.F. (Eds.), Large igneous provinces; continental, oceanic, and planetary flood volcanism. Geophysical Monograph vol. 100, American Geophysical Union, United States, pp. 95-122.

Sun, S.S., McDonough, W.F., 1989. Chemical and isotopic systematics of oceanic basalts: implications for mantle composition and processes. In: Saunders, A.D., Norry, M.J. (Eds.), Magmatism in the Ocean Basins. Geological Society Special Publications 42, pp. 313-345.

Sweeney, R.J., Duncan, A.R., Erlank, A.J., 1994. Geochemistry and petrogenesis of central Lebombo basalts of the Karoo igneous province. Journal of Petrology 35 (1), 95-125.

Sweeney, R.J., Falloon, T.J., Green, D.H., Tatsumi, Y., 1991. The mantle origins of Karoo picrites. Earth and Planetary Science Letters 107 (2), 256-271.

Tegner, C., Lesher, C.E., Larsen, L.M., Watt, W.S., 1998. Evidence from the rare-earth-element record of mantle melting for cooling of the Tertiary Iceland plume. Nature 395, 591-594.

Thy, P., 1985. Chemical diversity in basaltic glasses and the origin of ferrobasalts at oceanic spreading centers. Eos Transactions, American Geophysical Union, 66 (46), Fall Meeting Supplements, p. 1108.

Thy, P., 2003. Igneous petrology of gabbros from hole 1105A: oceanic magma chamber processes. In: Casey, J.F., Miller, D.J. (Eds.), Proceedings, Ocean Drilling Program Scientific Results, vol. 179. Ocean Drilling Program, College Station, TX, pp. 1-76 [Online].

Tuff, J., Takahashi, E., Gibson, S.A., 2005. Experimental constraints on the role of garnet pyroxenite in the genesis of high-Fe mantle plume derived melts. Journal of Petrology 46 (10), 2023-2058.

Ulmer, P., 1989. The dependence of the Fe^{2+}-Mg cation-partitioning between olivine and basaltic liquid on pressure, temperature and composition; an experimental study to 30 kbars. Contributions to Mineralogy and Petrology 101 (3), 261-273.

van Westrenen, W., Blundy, J., Wood, B., 1999. Crystal-chemical controls on trace element partitioning between garnet and anhydrous silicate melt. American Mineralogist 84 (5-6), 838-847.

Vuori, S.K., Luttinen, A.V., 2003. The Jurassic gabbroic intrusion of Utpostane and Muren; insights into Karoo-related plutonism in Dronning Maud Land, Antarctica. Antarctic Science 15 (2), 283-301.

Walter, M.J., 1998. Melting of garnet peridotite and the origin of komatiite and depleted lithosphere. Journal of Petrology 39 (1), 29-60.

Weaver, B.L., 1991. Trace element evidence for the origin of ocean-island basalts. Geology (Boulder) 19 (2), 123-126.

Wolmarans, L.C., Kent, K.E., 1982. Geological investigations in western Dronning Maud Land, Antarctica - a synthesis. South African Journal of Antarctic Research, Supplement 2. 93 pages.

Wooden, J.L., Czamanske, G.K., Fedorenko, V.A., Arndt, N.T., Chauvel, C., Bouse, R.M., King, B.W., Knight, R.J., Siems, D.F., 1993. Isotopic and trace-element constraints on mantle and crustal contributions to Siberian continental flood basalts, Noril'sk area, Siberia. Geochimica et Cosmochimica Acta 57 (15), 3677-3704.

Yaxley, G.M., Green, D.H., 1998. Reactions between eclogite and peridotite: mantle refertilisation by subduction of oceanic crust. Schweizerische Mineralogische und Petrographische Mitteilungen 78 (2), 243-255.

Yaxley, G.M., Sobolev, A.V., 2007. High-pressure partial melting of gabbro and its role in the Hawaiian magma source. Contributions to Mineralogy and Petrology 154 (4), 371-383.

Zack, T., Foley, S.F., Jenner, G.A., 1997. A consistent partition coefficient set for clinopyroxene, amphibole and garnet from laser ablation microprobe analysis of garnet pyroxenites from Kakanui, New Zealand. Neues Jahrbuch fuer Mineralogie.Abhandlungen 172 (1), 23-41.

Zhang, R.Y., Zhai, S.M., Fei, Y.W., Liou, J.G., 2003a. Titanium solubility in coexisting garnet and clinopyroxene at very high pressure; the significance of exsolved rutile in garnet. Earth and Planetary Science Letters 216 (4), 591-601.

Zhang, X., Luttinen, A.V., Elliot, D.H., Larsson, K. and Foland, K.A., 2003b. Early stages of Gondwana breakup; the $^{40}Ar/^{39}Ar$ geochronology of Jurassic basaltic rocks from western Dronning Maud Land, Antarctica, and implications for the timing of magmatic and hydrothermal events. Journal of Geophysical Research 108 (B9), 2449, doi: 10.1029/2001JB001070

Zimmer, M., Kroener, A., Jochum, K.P., Reischmann, T., Todt, W., 1995. The Gabal Gerf Complex; a Precambrian N-MORB ophiolite in the Nubian Shield, NE Africa. Chemical Geology 123 (1-4), 29-51.

Zolotukhin, V.V., Al'mukhamedov, A.I., 1991. Basalts of the Siberian Platform: distribution, mineral composition and mechanism of formation. In: Polyakov, G.V. (Ed.), Traps of Siberian and Deccan: similarities and differences. Nauka, Novosibirsk, pp. 7-39. (in Russian)

Zolotukhin, V.V., Al'mukhamedov, A.I., Tkachenko, N.A., 1991. Composition of main rock-forming minerals in Deccan and Siberian trap rocks: a comparison. In: Polyakov, G.V. (Ed.), Traps of Siberian and Deccan: similarities and differences. Nauka, Novosibirsk, pp. 140-177. (in Russian)